AN INVESTIGATION INTO A METHOD OF FAULT DETECTION ON LONG TRANSMISSION LINES USING MULTIPLE PROTECTION SCHEMES

A thesis submitted to

The Faculty of Graduate Studies

in Partial Fulfillment of the Requirements for the Degree

Master of Science

Department of Electrical & Computer Engineering

University of Manitoba

Winnipeg, Manitoba

Canada, R3T 2N2

by

Xun Yang

ISBN 0-315-81761-5

AN INVESTIGATION INTO A METHOD OF FAULT DETECTION ON LONG TRANSMISSION LINES USING MULTIPLE PROTECTION SCHEMES

BY

XUN YANG

A Thesis submitted to the Faculty of Graduate Studies of the University of Manitoba in partial fulfillment of the requirements of the degree of

MASTER OF SCIENCE

ACKNOWLEDGEMENTS

The research work described in this thesis was carried out by the author at the Department of Electrical Engineering, the University of Manitoba under the supervision of Dr. P.G. McLaren.

I would like to express my sincere thanks to Dr. Peter. G. McLaren, whom I admire, for his continuous advice, encouragement and guidance throughout the course of this work.

To Dr. W. W. L . Keerthipala , Dr. Rohitha Jayasinghe and Hong Man Yang and many other friends , whom I worked with in the same office, I would like to thank you for your assistance and especially for providing me with your programs and information.

Financial support for this work was provided by Manitoba Hydro and Dr. Peter G. McLaren. These assistances are gratefully acknowledged.

Finally, I wish to thank my parents for their encouragement and patience during the preparation of this thesis.

ABSTRACT

This thesis presents a recent research in the area of micro–processor relays for power transmission line systems. An investigation is made to the possiblity of a protection scheme based on the combination of three relaying algorithms in long line protection application. The theoretical background of the three algorithms (impedance measurement techniques, travelling wave correlation and wavefront prediction techniques) are introduced. Simulations based on a model transmission line system are performed in terms of each algorithm and the results are compared. A conclusion is given. A bibliography is included for reference.

CONTENTS

LIST OF FIGURES

Chapter 1
Introduction

1.1 GENERAL INTRODUCTION

The increase in the complexity of power systems has increased the need for fast protective schemes particularly on important lines. For years reductions in protective equipment operating times have been achieved by making improvements in relay designs and by the introduction of new technologies, such as digital techniques. When we examine the historical development in this area, we recognize two broad branches. The first utilizes digital computers to make better power frequency relays, while the second strives to extract information from transients to develop ultra–high–speed relay algorithms.

The conventional schemes continue to exploit basic physical principles introduced decades ago, namely current comparisons and impedance measurements. Relay operation is based on the measurement of power–frequency component parameters and therefore a relatively long time delay is required before adequate information is gathered about the various power–frequency quantities. Therefore, there is an inherent limit in such a system

to the increase in operation speed which cannot be overcome by improvements in relay design. These difficulties are more acute in the case of compensated lines. Great interest has always been shown in the so–called distance protective schemes which operate from measurements taken at the relaying point alone. The absence of communication links decrease cost and increase the speed of operation.

The emergence of UHV overhead lines and EHV cables in the modern bulk interconnected power systems presents some new and difficult problems to the conventional protective devices. These problems are caused by the transient behavior of the power system after fault inception. Transients in power systems are initiated by a sudden change in circuit conditions in which the system shifts from the steady state corresponding to the original conditions to a new steady state appropriate for the new conditions. This transition does not occur instantaneously but through an electrical transient, which is characteristic of the network and the event occurring. The conventional relays, e.g. distance relays, which assume that the electromagnetic transients are negligible, find difficulty in this situation when transient currents are comparably high. Hence the protection system must be designed to take account of such electromagnetic transients. Moreover, ultra–high–speed protection is necessary to reduce the fault time clearing and in turn reduce fault damage and improve power system stability. The use of fault initiated travelling–wave components in the protection of transmission lines can provide for faster relay operation. The above considerations are the reasons behind a recent interest in travelling–wave based schemes. Despite being all based on travelling–wave theory, each scheme has its own unique approach for fault detection and direction discrimination.

During the last few years, the development of fast microprocessor–based instrumentation with increased processing capabilities makes it possible to extract relaying information contained in the voltage and current transient components set up by the faults. These transients contain a wide spectrum of frequencies. The so–called travelling wave

protective schemes function by extracting information about faults from a broad–band of frequencies and should, in principle, be capable of fast operation time.

Perhaps the most thought–provoking technique for ultra–high–speed protection based on transients is the correlation technique which still serves as the basis for all the travelling wave distance protection schemes. It correlates the first wave approaching the fault from the relaying point and the corresponding wave reflected from the fault as it passes the relaying point, the maximum output of the correlation result corresponds to twice the distance to the fault.

The proposed scheme by this thesis stems from the available theories but tries to combine the advantage of each individual algorithm in a bid to achieve a better coverage of the protection over the transmission line. In practice, three different algorithms are applied to the same line system with a total length of over 500 km. It is known that the relationship between impedance and distance is linear for distance to fault for which a lumped parameter model is appropriate. Such a distance is typically around 150 km at power frequency. On long lines, say 500 km, the remaining part of the zone 1 coverage up to 400km requires a different technique for accurate measurement of distance particularly so around the 400 km boundary. A short window impedance measurement algorithm is employed to measure the impedance seen by the relay (Chapter 2) but we know it is only good for the first 150 km. The remainder of the zone up to 400km is covered by travelling wave distance measurement based on a correlation technique to recognize wavefronts returning from the fault [3]. (Chapter 3) Should the fault occur at a point on wave giving very low levels of wavefront on the line then a new waveshape prediction technique based on the telegraphers equations is used. (Chapter 4) It is equally applicable for any point on wave but computationally more complex than the correlation technique.

The proposed scheme is developed with reference to a transmission line model established using EMTDC. Then the theory is examined by different fault situations along

the transmission line. (Chapter 2, 3, 4) Then the characteristic features of the result of each algorithm are compared and a decision is reached (Chapter 5). The detailed description of the software is provided.(Chapter 6) A conclusion is given. (Chapter 7)

In this chapter, and before we briefly review some of the existing ultra–high–speed algorithm relays, it might be useful to mention some of the existing conventional relays which, until today, still play the main role in line protection.

1.2 DIGITAL DISTANCE PROTECTIVE RELAY ALGORITHMS

In all the distance protection algorithms the goal is to extract the apparent impedance, from the line terminal to the fault, by measuring the voltage and current at the line terminal. The impedance seen by a relay in such a case is proportional to the distance between the fault and the relaying point. The fault will be considered inside the protected zone if the measured impedance is less than say, 80% of the impedance of the protected zone in the healthy state. The basic equation relating the line impedance with the voltage and current measured at a relaying point is given by

$$\tilde{Z} = \tilde{V} / \tilde{I} \qquad (1.1)$$

where Z is complex and V and I are phasors. The digital estimation is fairly accurate and easy when both voltage and current are pure 60 Hz sinusoids. However, in the presence of transients the accurate estimation becomes very difficult.

Mann and Morrison [16] proposed one of the first algorithms for digital distance relaying. The method of calculation of line impedance involves the predictive calculation of peak current and peak voltage, the impedance being determined by division of peak voltage by the peak current. The peak voltage and current can be obtained through a very simple notion. A digital computer sampling a sinusoidal waveform can determine the peak values as follow:

$$v' = \omega V_{pk} \cos (\omega t)$$

$$v = V_{pk} \sin (\omega t)$$

$$v_{pk}^2 = v^2 + \left[\frac{v'}{\omega} \right]^2$$

$$\phi = \tan^{-1} \frac{\omega\, i}{i'} - \tan^{-1} \frac{\omega\, v}{v'}$$

(1 .2)

where i, i', v and v' are the instantaneous current and voltage sample and their derivative respectively and ω is the angular frequency of the sinusoid. The amplitude of the fault impedance is the ratio of the peak voltage amplitude to the peak current amplitude and the phase angle is the difference between the voltage and current phasors.

One computer based transmission line relaying system designed by Westinghouse was placed in experimental service. In order to reduce the effects of dc offset transients and subnormal frequency components caused by series capacitor banks during faults, they took the Mann and Morrison algorithm described above and modified it to use first and second differences, rather than raw sample values and first differences. Thus peak and phase values leads to:

$$v_{pk} = v'^2 + \left[\frac{v''}{\omega} \right]^2$$

$$\phi = \tan^{-1} \left(\frac{\omega\, i'}{i''} \right) - \tan^{-1} \left(\frac{\omega\, v'}{v''} \right)$$

(1 .3)

It is obvious that this algorithm amplifies the high frequency noise and in return will greatly affect the result if the signals are not pre–filtered properly.

Sachdev et al. [7] developed a digital distance relay which uses least square filters. The algorithm explicitly filters decaying exponential components and some harmonics, determines the real and imaginary components for the fundamental frequency current and voltage phasors and calculates the impedances as seen from the relay location. It suggested

that the voltage and current waveforms presented to the relay during the fault consist of decaying exponential, fundamental frequency and high frequency components. For example the voltage waveform after a fault can be approximated by

$$v(t) = k_0 \exp^{-(\frac{t}{\tau})} + k_1 \sin(\omega_1 t + \theta_1) + k_2 \sin(\omega_2 t + \theta_2) \quad (1.4)$$

Seven samples of voltage are needed in order to solve the above equation in terms of real and imaginary components. The real and imaginary components of a voltage and a current then can be used to calculate the real and imaginary components of the impedance seen at the relay.

Another group of algorithm was going on in parallel to the above group of algorithms. These algorithms are based on the lumped parameter representation of the transmission line by a set of first order linear differential equation of the form:

$$V = Ri + L\frac{di}{dt} \quad (1.5)$$

McInness and Morrison [16] proposed a solution for R and L parameters by integration of the above equation over two successive time periods and solution of the resulting simultaneous linear equations. The integrations are performed numerically using the trapezoidal rule:

$$\int_{t1}^{t2} Vdt = R\int_{t1}^{t2} idt + L\,|\,I(t2) - I(t1)\,|$$
$$\int_{t3}^{t4} Vdt = R\int_{t3}^{t4} idt + L\,|\,I(t4) - I(t3)\,| \quad (1.6)$$

An advantage of using an R–L line model is that the d.c offset current is considered a valid fault component in the solutions. This is however valid only for short to medium length lines where the shunt capacitance is small and can be neglected.

In the algorithm by Smolinski [7], the line model includes the shunt capacitance. A single Π type circuit is used to model the transmission line from the relay location to the fault. The voltage and current at the relay location can be shown to satisfy:

$$V = Ri + L\frac{di}{dt} - RC\frac{dv}{dt} - LC\frac{d^2v}{dt^2} \qquad (1.7)$$

Four successive sets of voltage and current samples are required to solve the four unknown, R, L, RC and LC.

McLaren and Redfern [12] are among many who recognized the presence of the transients but continued the effort to extract and utilize the 60 Hz components. The fundamental voltage and current components were extracted by a fourier–series processor and then were used to provide an impedance value for the system as seen at the relaying point. The result indicate that the filter characteristics of the fourier–series processor, although not ideal, nonetheless gave considerable rejection of non–fundamental signals in the time available (typically one cycle).

A method of transmission line protection based on the use of the wave equation model of the line was developed by Vitins[4]. The author proposed the decomposition of the measured signals at the relay station into the two travelling wave functions:

$$F_1(t) = V(t) + Z_0 I(t)$$
$$F_2(t) = -V(t) + Z_0 I(t) \qquad (1.8)$$

where Z_0 is the surge impedance of the line. It will be shown briefly in the next section and in detail in the chapter 3 that F_1 and F_2 are proportional to voltage waves which move in opposite directions along the line. The fault distance appears as a time delay between these two functions at the measurement site. Under steady state conditions and in quasi–stationary steady state following the inception of a fault, F_1 and F_2 are the phasors. After the fault–produced transient has died out, the phase angle between F_1 and F_2 is proportional to the fault distance. The algorithm recognizes the presence of travelling waves from the

occurrence of a fault in the power system, but its detection method is based on the estimation of a 60 Hz signals.

1.3 LINE PROTECTION BASED ON TRANSIENTS

The algorithms described in the above section use low pass filters to attenuate the high frequencies generated by transients. Such transients still have a substantial influence on 60 Hz relays in spite of this. Attempts which have been made to increase the impedance relay speed and accuracy, show that an attempt to make an impedance relay faster inevitably makes for a less accurate impedance measurement because of the transient phenomena accompanying the fault. The best detection time that can be achieved by the algorithms discussed so far is probably no less than 20 ms for faults at the boundary.

The need to improve fault clearance times and the development in digital techniques has motivated several authors to consider transient relaying approaches. The common feature of these algorithms is that they act on the transient–produced superimposed signals and the transmission line is represented by a distributed parameter line model.

The use of transient superimposed signals constitutes the basis of this approach. The inception of a fault in a transmission line will cause the post fault voltage and current at the relaying point to deviate from the steady state pre–fault voltage and current respectively. Hence we can write

$$V(t)_{post\text{-}fault} = V(t)_{pre\text{-}fault} + \Delta V(t)$$

$$I(t)_{post\text{-}fault} = I(t)_{pre\text{-}fault} + \Delta I(t) \qquad (1.9)$$

where $\Delta V(t)$ and $\Delta I(t)$ denote the fault generated voltage and current deviation from pre–fault steady state signals as the function of time. These incremental signals are appropriate for high speed distance protection as they contain all the information regarding

the travelling waves injected by the fault. Under normal, unfaulted, steady state conditions the incremental quantities are zero except for the presence of noise. In a distributed parameter model representation of a transmission line, the relationship between voltage, current, time and distance is fully described by the telegraph equation. If the losses are negligible, it reverts to the well–known wave equation:

$$-\frac{\partial e(x,\ t)}{\partial x} = l\,\frac{\partial i(x,\ t)}{\partial t}$$

$$-\frac{\partial i(x,\ t)}{\partial x} = c\,\frac{\partial e(x,\ t)}{\partial t} \qquad (1.10)$$

where l and c are the inductance and capacitance per unit length. D'Alembert's solution to the wave equation, in terms of forward and backward travelling wave can be expressed as

$$e(x,\ t) = f_1(x - ut) + f_2(x + ut)$$

$$i(x,\ t) = \frac{1}{Z_0}\left[f_1(x - ut) - f_2(x + ut)\right] \qquad (1.11)$$

where Z_0 is the characteristic impedance of the line and u is the surge velocity. The backward and forward travelling wave functions in terms of incremental signals can be represented as

$$S1(t) = 2f_2(t) = \Delta V(t) - Z_0\,\Delta I(t)$$

$$S2(t) = 2f_1(t) = \Delta V(t) + Z_0\,\Delta I(t) \qquad (1.12)$$

S1 is the backward wave function, equal to twice the voltage wave moving in the negative direction and S2 is the forward wave function, equal to twice the voltage wave moving in the positive direction. The travelling wave theory and the travelling wave distance protection scheme will be discussed in detail in chapter 3.

Applications in this field can be generally categorized into directional, phase selection and distance relay algorithms.

1.3.1 DIRECTIONAL COMPARISON SCHEME

Directional detector is intended for use with a transfer trip carrier communication channel, i.e. with minimum communication requirements. Most of the algorithms for detecting fault direction will make use of the modal components of the voltages and currents which are caused to be superimposed upon the steady state pre–fault power frequency components following the fault inception.

In the relay by Dommel and Michels [6,7], a directional discriminant function D was proposed. The discriminant is a function of the fault initiated travelling wave characteristic and its derivative with respect to time. The changes in current and voltage signals composing this wave characteristic are measured as differences from steady state reference values. The directional discriminant travelling wave function is zero for backward faults and a known constant for faults in the forward direction. This discriminant is described as follows

$$D\ (\ t\ ) = \left[\ \Delta V - Z_0\ \Delta I\ \right]^2 + \frac{1}{\omega^2}\left[\ \frac{d}{dt}\ \Delta V - Z_0\ \frac{d}{dt}\ \Delta I\ \right]^2 \qquad (1.13)$$

where Δ V and Δ I are the incremental voltage and current signals measured at the relaying point respectively. Z_0 is the line surge impedance and ω is the fundamental power component angular frequency. The function D (t) is independent of the fault inception angle and the line termination. The above equation can be rewritten as a function of the backward S1 signal as in equation :

$$D\ (\ t\ ) = S1^2 + \frac{1}{\omega^2}\left[\ \frac{d}{dt}\ S1\ \right]^2 \qquad (1.14)$$

For reverse faults with respect to the relaying point, the travelling wave discriminant function remains zero (D (t) = 0) for a time equal to twice the travel time of the protected line. For a forward fault, under the assumption of a lossless line, the travelling wave discriminant evaluated at the relay point will remain constant from the time when the first

wave is sensed to the time when its reflection comes back from the fault point for an internal fault or from the opposite end for an external fault. The algorithm is designed to operate in a directional comparison scheme which requires a carrier communication channel between both ends of the line. Also, it is worth mentioning that although the discriminant function is independent of the fault inception angle, it depends on the properties of the power frequency voltage profiles that follow the wavefront.

In 1980 Vitins [4] presented a relaying technique based on the fault trajectory of the scaled current deviation against the voltage deviation. The proposed technique can be represented by fig 1.1. The deviation signals ΔV and ΔI measured at the relay location were given by

$$\Delta V(t) = \frac{X_{s1}}{X_{s1} + X_{L1}} E \cos(\omega t + \theta)$$

$$\Delta I(t) = \frac{1}{X_{s1} + X_{L1}} E \left[\sin(\omega t + \theta) - \sin\theta \right] \qquad (1.15)$$

where θ is the fault inception angle and the protected line is represented by lumped parameters.

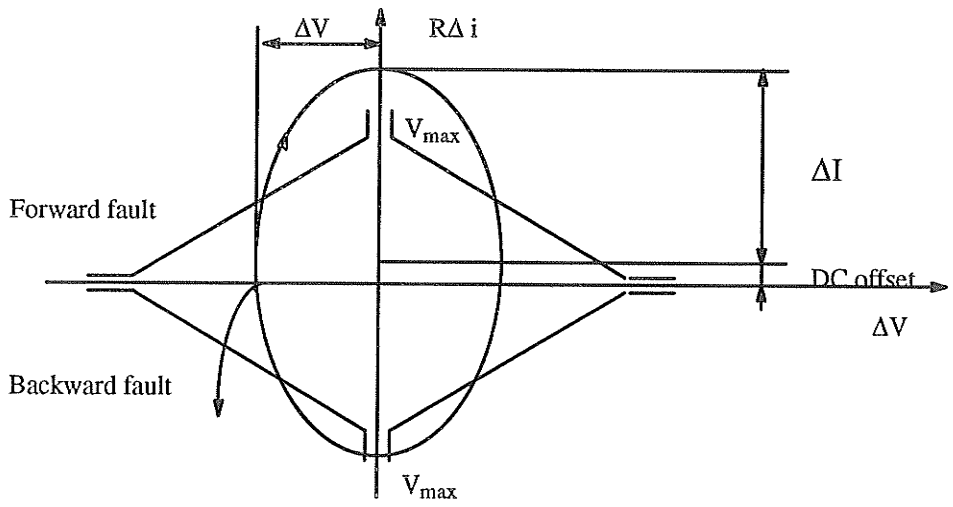

Figure 1 .1 : trajectory

Figure1.1 shows the typical boundary presented by the author for forward and backward faults. A replica resistance R introduced in the current deviation signal path leads to a replica voltage deviation ΔV_R. An initial excursion into the first or third quadrant means a reverse fault(the trajectoy goes clockwise), while an initial excursion into the second or fourth quadrant indicates a forward fault (the trajectory goes anti–clockwise). This information is exchanged with the relay at the opposite end of the protection zone. If the combination of the locally detected direction and the information from the opposite relay indicates a fault inside the protected zone, a trip signal is issued. Lanz, at. el. [17] described the use of replica impedance Z_R in the current circuit in the subsequent studies. This produces a phase shift between ΔV_R and ΔI equal to the source impedance angle and in turn the fault trajectory becomes a straight line. Sometimes, the travelling wave components of higher frequency may cause brief excursions of the trajectories into quadrants which do not correspond to the actual direction of the fault. To confirm the directional decision, the use of an averaging function is suggested.

$$F(\tau) = \int_0^{\tau} \Delta V(t)\, \Delta V_R(t)\, dt \qquad (1.16)$$

The function F(τ) is continuous and always lies in the negative half of the plane for faults in the forward direction and in the positive half for faults in the reverse direction.

Johns and Aggarwal [5,10], presented a directional comparison scheme in conjunction with a carrier communication channel. The sequence in which the derived fault–initiated forward and backward wave characteristics exceed a given threshold was used to detect the fault and determine its direction. The operating principle of this algorithm can be conveniently explained by considering the travelling wave functions S1 and S2 described by equation 1.12. S1 is the voltage wave moving in the backward direction and S2 is the voltage wave moving in the forward direction. As mentioned above, for a fault in the backward direction and during a time equal to twice the travel time of the protected line 2τ,

$$S1 > 0$$

$$S2 = 0$$

In a multi–conductor line, the modal transformation matrix is used to decouple the phase signals into modal signals.

1.3.2 FAULT CLASSIFICATION AND PHASE SELECTION

Single pole autoreclosure applications demand reliable phase selection. In ultra–high–speed protection the need for ultra–high–speed phase selection becomes very necessary. Faulted phase selection, and hence selective pole tripping, is an important relaying capability because it increases the system stability as well as its availability. Therefore fault classification as a relaying feature also enhances the protection scheme.

Crossley described a method of selecting the phase or phases involved in the fault. In his method, the changes in the voltage and current signals caused by the disturbance are converted into their frequency components by a Fourier transform based on a one cycle window. The magnitude of the frequency components of the incremental voltage and current signals are evaluated at four chosen frequencies as:

$$K_V = \frac{1}{4}\left[\,|V(0)| + |V(\omega)| + |V(2\omega)| + |V(3\omega)|\,\right]$$

$$K_I = \frac{1}{4}\left[\,|I(0)| + |I(\omega)| + |I(2\omega)| + |I(3\omega)|\,\right] \qquad (1.17)$$

where $\omega = 2\pi f$ and f is the system frequency. The time varying current criterion K_I is compared against the voltage criterion K_V. When the locus exceeds a pre–determined admittance threshold the faulted phase or phases are confirmed. The operation time was found to be 2 to 5 ms depending on the fault type and location.

Mansour and Swift [9] presented a faulted phase selection and fault classification algorithm. Two discriminant functions derived from the forward and backward travelling waves and their differentiation are used to construct a table based on a transformation matrix

used to decouple the phase signals into their respective modal signals. The forward discriminant function for earth and aerial modes are

$$D_{F0} = S2_0^2 + \frac{1}{\omega^2}\left[\frac{d}{dt} S2_0\right]^2$$

$$D_{F1} = S2_1^2 + \frac{1}{\omega^2}\left[\frac{d}{dt} S2_1\right]^2$$

$$D_{F2} = S2_2^2 + \frac{1}{\omega^2}\left[\frac{d}{dt} S2_2\right]^2 \qquad (1.18)$$

Calculating the value of these discriminant functions for certain faults but with different phases as a basis, the fault can be classified and the faulted phase can be selected. More details will be discussed in Chpater 4.

1.3.3 TRAVELLING WAVE DISTANCE PROTECTION

Estimating the location of the transmission line faults has been a subject of interest for many years. The major reason for this activity is that a good estimate can reduce the time required for repairing the damage caused by the fault and for restoring service to customers. The prototype of the algorithm was first proposed in 1977 by Takagi by developing a current differential carrier relay based on travelling wave theory. The relay simply compares the current entering and leaving the protected zone. During normal operation or on occurrence of an external fault the currents at the two ends of the protected zone are equally apart from the travel time delay τ. For an internal fault the currents become unequal and their differences exceeds a threshold which should then lead to the initiation of a tripping signal. This can be explained by assuming that the voltage and current values from both line terminals are available. Two functions can be formed at both line ends(say R and S). These two functions for an external fault satisfy the following relation:

$$S1(t)\,|_R = S2(t-\tau)\,|_S$$

$$S1(t)|_S = S2(t-\tau)|_R$$

where τ is the time taken for a wave to propagate from one line end to the other. The above equations can be rewritten in discrete form as:

$$\epsilon(t)|_R = \frac{1}{Z_0}\left[S1(t)|_R - S2(t-\tau)|_S \right]$$
$$\epsilon(t)|_S = \frac{1}{Z_0}\left[S1(t)|_S - S2(t-\tau)|_R \right] \qquad (1.19)$$

In the case of a perfectly modeled lossless transmission line, the function $\varepsilon(t)|_R$ and $\varepsilon(t)|_S$ are zero in the absence of an internal fault. In practice a specified threshold level is set on the difference function. When an internal fault does occur the above two functions become non–zero. In a three phase line the algorithm required modal decomposition of the phase voltage and current measured at both line ends.

A major disadvantage with the scheme is the requirement for a wide bandwidth data communication channel between the ends of the protected line.

Ibe and Cory [18] presented an accurate method of fault location in transmission lines using the telegraph equations as a line model. The voltage and current samples taken at one end of a line within the first 5 ms after fault inception were used to generate instantaneous voltage and current profiles for the rest of the transmission line.

Different criteria functions, involving the computed variables were applied to determine the fault positions. The basic functions F(x) involve any one of the square of the voltage, the square of the current or the product of the two. The squared voltage function is

$$F(x) = \frac{1}{T - 2x/u} \int_{x/u}^{T-x/u} V^2(x, t)\, dt \qquad (1.20)$$

where T is the window duration, u is the propagation velocity and x is the discrete point on the line at which the voltage V is calculated and goes from zero to the protected line length.Fault position is determined by the turning point in the F(x) function. Since a fault

position is indicated by the turning point of F(x), the variation of the tangent amplifies this sudden change in its shape.

$$G\ (\ x\ ) = \frac{d^2\ F\ (\ x\ )}{dx^2} \qquad (\ 1\ .21\ )$$

The result shows that the peak of the function G (x) determines the fault position. In a three phase system a transformation matrix is used to decouple the three phase signals into three independent modal signals.

In 1980, a single ended travelling wave protective relay was described by Ko [19]. The algorithm is based on the travelling wave functions S1 and S2 . The fault location is estimated by detecting the first wave in the S2 signal arriving at the fault locater. The observation time corresponds to twice the transit time of the protected zone length. The fault reflected wave is recognized by calculating the first or second derivative with respect to time of the S1 signal. This scheme may mal–operate if there is more than one discontinuity point in front of the relay. Moreover such mal–operation may occur even due to the reflection from the remote end of the protected line.

Corssley and McLaren[1,11] presented a distance protection technique based on travelling wave theory. The authors used, for the first time, a cross–correlation function to recognize the initial wave reflected from the fault. The direction to the fault is detected first by the sequence in which the forward S2 and backward S1 directional relaying signals exceed a pre–determined threshold. For a detected forward fault, a section of S2 relaying signal representing the wavefront is stored and cross–correlated with subsequent sections of waveform on the S1 signal as follows:

$$\Phi_{S1,S2}\ (\ m\ \Delta t\ ) = \frac{1}{N} \sum_{k=1}^{N} S1\ (\ k\ \Delta t + m\ \Delta t\ )\ S2\ (\ k\ \Delta t\ ) \qquad (\ 1\ .22\ )$$

The cross–correlation reaches a maximum when the S1 section is similar to the stored section of S2. The time delay to reach this maximum corresponds to twice the distance

between the measuring point and the fault position. In order to obtain meaningful correlation, the authors suggested that the correlation to be performed between sections of S2 and S1 from which the mean value has been removed.

In a three phase system, a Wedepohl transformation matrix for a fully transposed transmission line was used to decouple the phase signals into their respective modal signals. The performance of this technique was tested for a two terminal transmission line and some limitations were reported, such as the influence of the reflection from the remote end, close–up faults when cross–correlation output is a uni–directional and discrimination between internal and external faults.

1.4 SUMMARY

As mentioned above, both travelling wave relays and impedance measurement relays have their advantages and disadvantages. For impedance measurement relay, the way to efficiently eliminate non–power frequency components is still not accurate enough. There are many factors which affect the accuracy of fault location, introducing substantial errors in measurements of the reactance between the line terminal and the fault such as the fault resistance, pre–fault load current and transient errors of current transformers. One other flaw is the system model itself, because as the line goes beyond a certain length, say 150km, the distributed parameters are not negligible and thus will greatly affect the results of impedance measurement. Moreover some problems are associated with certain transmission lines such as the long series compensated line.

The traveling wave relay has a number of practical limitations as well, such as those imposed by the bandwidth of conventional transducers, the presence of noise, very high sampling rate requirements in the digital processors and the dependence of the presence of travelling wave components on system and fault conditions. The problems get a little bit serious in the case of close–up faults and those near voltage zero. There could, however, be

an advantage in long–line applications, where the travelling waves persist for much longer times by virtue of the lower–frequency phenomenon associated with such lines.

One other advantage of the travelling wave relaying schemes over the conventional methods is that the effects of load current are reduced to a minimum, and in some of them, the UHS feature (i.e. relay decision time of a quarter cycle or less) is achieved. However each of the developed or suggested travelling wave schemes up till now has its own potential limits or problems.

In general the available relaying algorithms cannot stand alone but must complement the existing relays where they are in difficulty. One would imagine an ideal relay which embrace the following features:

1. Minimum communication requirements between the protected ends.
2. Independence of fault initiation angle.
3. Faulted phase selection and fault classification capability.
4. Ultra–high–speed fault clearance.
5. Insensitivity to parameter variation and different system configurations

The potential limits of the available schemes represent the motivation of this present study. The relaying system described here is intended to include as many of the mentioned capabilities as possible .

1.5 DORSEY FORBES CHISAGO TRANSMISSION LINE

The line used for this study is the 500kV transmission line from Dorsey to Forbes and Chisago. The two parts of the 500kV line system were placed in commercial operation in September, 1979 and May, 1980. It was jointly constructed by Manitoba Hydro, Northern States Power and Minnesota Power. The transmission line system connects the three companies. The southern section of the system is 220km long and connects Northern States Power's Chisago County Substation to Minnesota Power's Forbes Substation. The northern

section of the system is 538km long and connects Manitoba Hydro's Dorsey HVDC Converter Station to the Forbes Substation. This was the longest single–phase switched section of 500kV transmission line in the world at one time [15]. The excessive generation in Manitoba in summer time can compensate the summer peak situation for Northern States Power while in the winter, Northern States Power does the opposite, since the lakes are frozen in Manitoba. The Dorsey–Forbes–Chisago line is transposed along the route in order to yield more equal phase–to–phase capacitive coupling.

There are 4 transposition points on the line which is 538km long. Transposition points 4,5,6 and 7 are at distances from Dorsey of 88,191,324 and 444 km respectively. A model of the Dorsey–Forbes–Chisago 500kV transmission line system is simulated by using the EMTDC program.

The system model can be seen in Fig 1.2

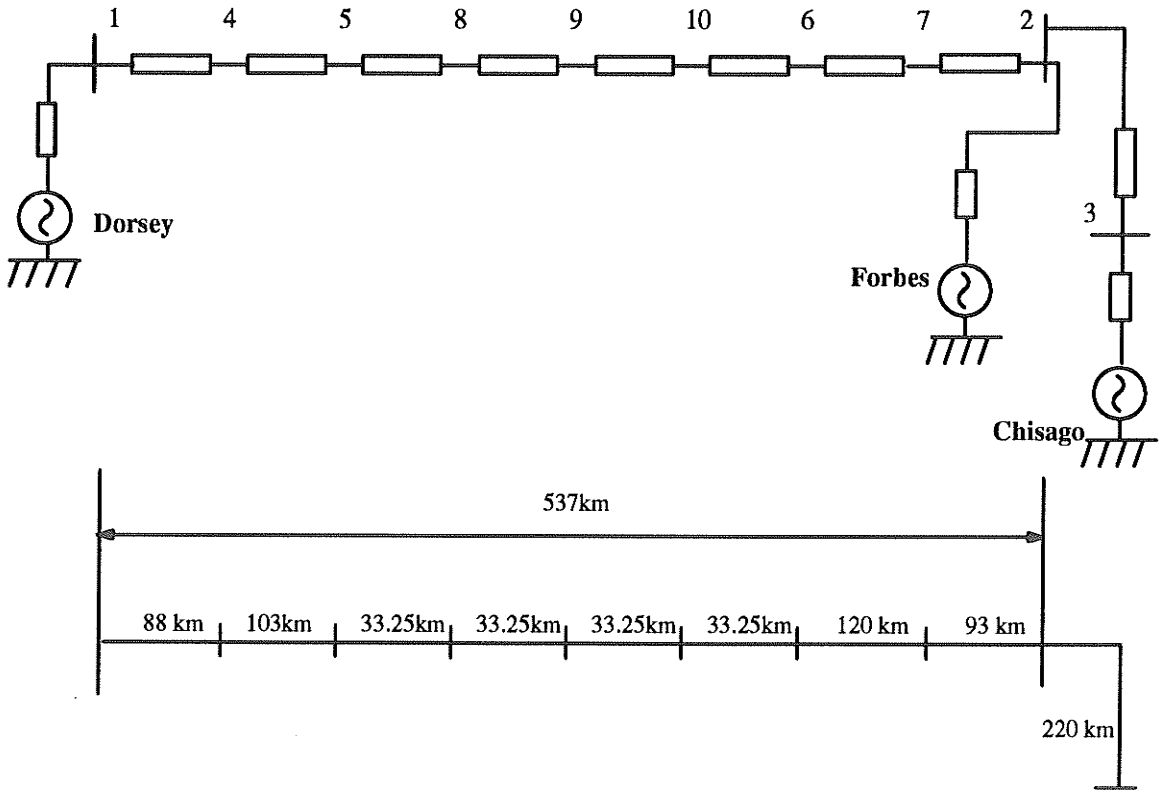

Figure 1 .2 : Dorsey–Forbes–Chisago Transmission Line System

In this model, the whole transmission line is segmented into virtually 9 sections which is more than only the transposition points so that we can take a closer look at how the proposed algorithm works at different locations along the line. We labeled the starting point of each section as 4, 5, 8, 9, 10, 6, 7, 2 and 3 which are 88, 192, 225, 258, 291, 324, 444, 537, 664 km from Dorsey respectively.

The reason for cutting the transmission line into so many fragments is for the easy analysis of different algorithms we will apply in the later chapters. The total length of the transmission line is 537 km from dorsey substation to Chisago. According to the requirement of the EMTDC simulation program, each segment is separated by nodes. Each node has an internal structure of the following diagram:

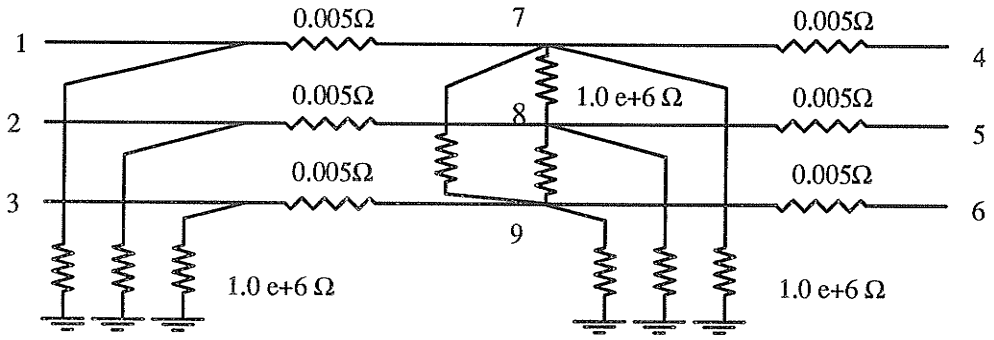

Figure 1 .3 : substation diagram for transmission line system

In the diagram, numbers from 1 to 9 represent different positions in the node and we can see resistors are used to connect these positions. It's obvious that we can imitate all sorts of fault situations by setting the corresponding phase to ground or phase to phase resistance to zero. We will use this method to generate faulted signals for testing throughout this study.

Chapter 2
Short Window Impedance Measurement

2.1 INTRODUCTION

This chapter is concerned with the algorithms which can be traced back to almost three decades ago, namely, the impedance measurement algorithm. The essence of the technique is to operate on the samples of voltage and current to produce estimates of the parameters at power frequency for protection. In this particular application, we consider them as the fundamental frequency voltage and current phasors.

The following algorithms are generally regarded as appropriate tools for application in this field:

1. Fourier Algorithm:

In its simplest form a Fourier Algorithm extracts the fundamental frequency phasor from samples for a periodic signal taken at equal intervals over a full period of the signal. It is equivalent to one term of the Discrete Fourier Transform and has been

represented as the convolution of samples of a reference sinusoid and a reference cosinusoid with the input signal. Taken over a full period, the Fourier calculation rejects harmonics of the fundamental frequency. The introduction of FFT (Fast Fourier Transform) further makes it possible to implement this technique on a real time basis and also it can be modified to work for intervals of less than a full period [3].

2. Walsh Type Algorithm:

The Walsh function algorithms are closely related to the Fourier algorithms except for the use of periodic square waves rather than sinusoids and cosinusoids. The convolution mentioned above is simplified because the sample values of the reference square waves are either plus or minus in sign. Several of the square wave signals must be used, however, to obtain the desired sinusoidal components.

3. Curve Fitting Algorithm:

Curve fitting algorithms [7] attempt to fit some parameterized representation of the signal to the measurements. Parameterizations include polynomials, trigonometric series, and mixtures of trigonometric and exponential functions.

To do this, a model of the system must be established. In particular a series R–L model of the faulted line implies that the terminal voltage and current must satisfy a first order linear differential equation. The parameters of interest for relaying are the values of R and L which must be estimated from the waveforms in the system model .

2.2 SHORT WINDOW ALGORITHM

Among the above mentioned algorithms, the Fourier series analysis offers more desirable benefits than the others in terms of simplicity and performance, and thus is preferred by research engineers. By definition, the Fourier–series analysis of a waveform

f(t) which is periodic over the period T is

$$f(t) = a_0 + \sum_{n=1}^{\infty} C_n \cos(n\omega t - \phi_n) \qquad (2.1)$$

where

$$c_n = \sqrt{(a_n^2 + b_n^2)}$$

$$\phi_n = \tan^{-1}\left(\frac{b_n}{a_n}\right) \qquad (2.2)$$

and

$$a_n = \frac{2}{T}\int_0^T f(t)\sin(n\omega t)\,dt$$

$$b_n = \frac{2}{T}\int_0^T f(t)\cos(n\omega t)\,dt$$

$$\omega = \frac{2\pi}{T} \qquad (2.3)$$

This process separates the d.c. fundamental and harmonic components of f(t) and we know that the fundamental frequency components are a_1 and b_1, respectively.

The continuous integrals of eqn. 2.3 are not directly suitable for processing. The input waveforms f(t) are sampled at N samples per system cycle, and the integral is taken over the system period which immediately precedes the sampling instant in question. The processor extracts the fundamental components of these inputs and uses eqn. 2.3 in its discrete form:

$$a_1 = \frac{2}{N} \sum_{k=0}^{N-1} f(t-k) \cos\left(\frac{2\pi}{N} k\right)$$

$$b_1 = \frac{2}{N} \sum_{k=0}^{N-1} f(t-k) \sin\left(\frac{2\pi}{N} k\right)$$

(2.4)

or in a more general way

$$X_n = \sum_{k=0}^{N-1} x_k \, e^{-j\left[\frac{2\pi n k}{N}\right]}$$

(2.5)

where X_n is the frequency component which is a complex number, and x_k is the individual sample within the sample window. This equation is commonly referred to as DFT (Discrete Fourier Transform).

When $N \rightarrow \infty$, $A_1 \rightarrow a_1$, $B_1 \rightarrow b_1$, and eqn. 2.4 will converge to eqn 2.3. The sampling rate N, is chosen to be at least twice that of the greatest noise frequency likely to be present in the input waveforms f (t). If there is any conflict between this and the processor's maximum sampling rate, a low–pass filter can be inserted before the processor input, but this will cause the loss of response speed.

Using the system represented in the block diagram shown in Fig. 1, the magnitude and phase angle of the fundamental component of an input waveform can be calculated with respect to the reference waveforms cos(2π n / N) and sin (2π n / N). For any input wave form, we can obtain:

$$C_1 = \sqrt{(A_1^2 + B_1^2)}$$

$$\phi_1 = \tan^{-1}\left(\frac{B_1}{A_1}\right)$$

(2.6)

Using the above equation, the voltage and the current phasors can both be obtained from the sampled voltage and current waveforms. The system impedance can be derived by

dividing the two phasors. i.e.

$$\tilde{Z} = \frac{C_V}{C_I}$$

$$\phi_Z = \phi_V - \phi_I$$

(2 .7)

The above computation is carried out at each sampling interval, and gives a value of Z based on the previous cycle of the voltage and current waveform.

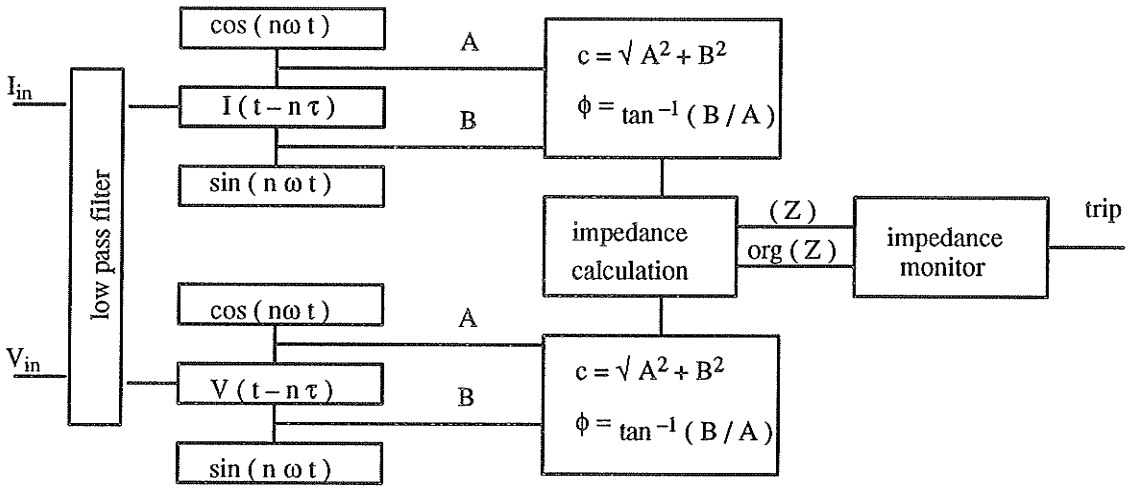

Figure 2 .1 : fourier analysis impedance measurement scheme

When using the Fourier Transform, the aliasing effect during waveform sampling should be avoided since it introduces errors in the transform process. It is known that the spectrum of a sampled waveform consists of shifted replicas of X (ω) at the harmonics of the sampling frequency f_s. If the sampling frequency is less than the highest significant frequency component in the original waveform, the shifted replicas will overlap with each other. This spectral overlap is called aliasing. In order to avoid higher frequency interference, an anti–aliasing filter can be used. This is a low–pass filter which physically filters out the frequency components above f_s / 2 before sampling.

To improve the speed and to reduce the influence from travelling wave transients, a short window algorithm is suggested[10]. One other reason for this is that the concept of power frequency impedance is no longer suitable when the window contains both pre and post fault signals. The shortened window implies that we are extracting impedance at a frequency higher than the fundamental frequency provided that the impedance we obtain still satisfy the basic equation

$$v\ (\ j\omega_e,\ t\ )\ =\ R\ i\ (\ j\omega_e,\ t\ )\ +\ L\ i'\ (\ j\omega_e,\ t\ ) \qquad (2.8)$$

where ω_e is the extraction frequency. According to [2], the R and L can be considered to be constant up to a frequency of 250Hz for a 500 kV line. ω_e can be any value below this upperbound. In practice, the short window R,L algorithm uses a 12.5 ms window length for both voltage and current. If V_{r1}, i_{r1} and V_{r2}, i_{r2} are the real and imaginary parts of the voltage and current phasors from this short window Fourier analysis, then the algorithm solves the two unknowns R and L:

$$\begin{bmatrix} R \\ L \end{bmatrix} = \frac{1}{D\ (\ t\ )} \begin{bmatrix} i'_{r2} & -i'_{r1} \\ -i_{r2} & i_{r1} \end{bmatrix} \begin{bmatrix} V_{r1} \\ V_{r2} \end{bmatrix} \qquad (2.9)$$

where $D(\ t\ ) = i_{r1}\ i_{r2}' - i_{r1}'\ i_{r2}$

The derivatives are calculated using a three–sample window.The measured resistance and reactance applicable to any sample instant k are determined from equation 2.9 which, when written in discrete form, yields R(k), X(k) as follows:

$$R\ (\ k\ )\ =\ \left[\ v_{r1}\ (\ k\ )\ i'_{r2}\ (\ k\ )\ -\ v_{r2}\ (\ k\ )\ i'_{r1}\ (\ k\ )\ \right]\ /\ D\ (\ k\ )$$

$$L\ (\ k\ )\ =\ \left[\ v_{r2}\ (\ k\ )\ i_{r1}\ (\ k\ )\ -\ v_{r1}\ (\ k\ )\ i_{r2}\ (\ k\ )\ \right]\ /\ D\ (\ k\ ) \qquad (2.10)$$

where

$$D(k) = i_{r1}(k)\, i'_{r2}(k) - i'_{r1}(k)\, i_{r2}(k) \qquad (2.11)$$

The differential current terms $i'_{r1}(k)$, $i'_{r2}(k)$ in equation 2.9 are usefully approximated by assuming piecewise linearity between current samples so that, in terms of immediately preceding samples ($i_{r1}(k-1)$, $i_{r2}(k-1)$), they are replaced by

$$i'_{r1}(k) = \left[i_{r1}(k) - i_{r1}(k-1) \right]$$

$$i'_{r2}(k) = \left[i_{r2}(k) - i_{r2}(k-1) \right] \qquad (2.12)$$

The impedance can be easily found to be

$$Z = R(k) + jX(k) \qquad (2.13)$$

where

$$X(k) = \omega L(k)$$

and thus the impedance trajectory can be established on the X – R plane.

The familiar R–jX impedance plane is a convenient tool for visualizing the results of these calculations. Computed values of impedance for various fault and non–fault conditions are plotted on the plane and compared with each characteristic.

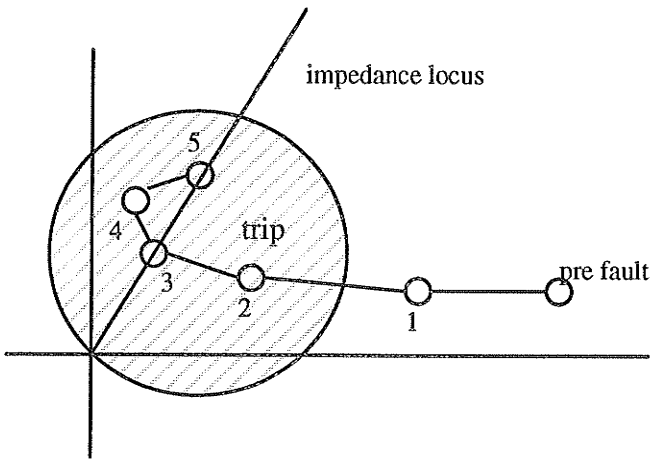

Figure 2 .2 : mho relay characteristics

Figure 2.2 shows the familiar mho circle which describes the zone of protection for many conventional distance relays, along with a line representing the locus of short–circuit impedances for faults along the protected transmission line. The mho circle under–reaches the remote terminal so that the relay provides zone 1 or local backup non–pilot tripping. The numbered marks represent a time sequence of computed impedance values, beginning with a value computed entirely from pre–fault voltage and current samples, this does not normally represent a real impedance element of the system, but rather an apparent impedance resulting from load flow conditions, the particular pre–fault point corresponds to real power flow away from the bus where the digital relay is located.

2.3 RESPONSE TO FAULT CONDITIONS

The Fourier–series processor extracts the fundamental component which can be used to provide an impedance value for the system as seen at the relaying point. For power system fault waveforms, there are exponentially decaying d.c. components. transient harmonic and non–harmonic frequency signals. Also, for the transition period after fault incidence the processor uses both pre–fault and post–fault information. To investigate the behavior of the processor with these wavefoms, a computer simulation has been used.

Input waveforms were generated from the EMTDC program using the line model illustrated in chapter one. Single phase to earth faults and three phase to ground faults were simulated for fault incidence at various locations along the line with variable fault resistance. The sampling rate chosen was 64 samples per cycle, equivalent to 3.84 kHz on a 60 Hz system. The input waveforms I_{in} and V_{in} are sampled at the rate of 60N per second. Each sample is fed into an N–element array which holds the sample history of the previous N samples. As each new sample is entered into the first location of this array, all previous samples shift one element to the right, and the sample at the Nth element is discarded. The N elements of this array are then sent through the short window fourier transform with

cos($\omega k \tau$) and sin ($\omega k \tau$). From the result the corresponding current and voltage phasors are obtained and the system impedance is calculated by the matrix multiplications.

Fig 2.3 depicts the typical voltage and current waveforms for 3 phase to ground fault and Fig 2.4 represents single phase to ground fault, respectively. We can see at the 0.03 second instant the fault happens, and after a short transient period, the voltage and current begin to converge on their postfault values. These are the signals we are going to use in our algorithm and our task is to find out the change in the impedance during this period.

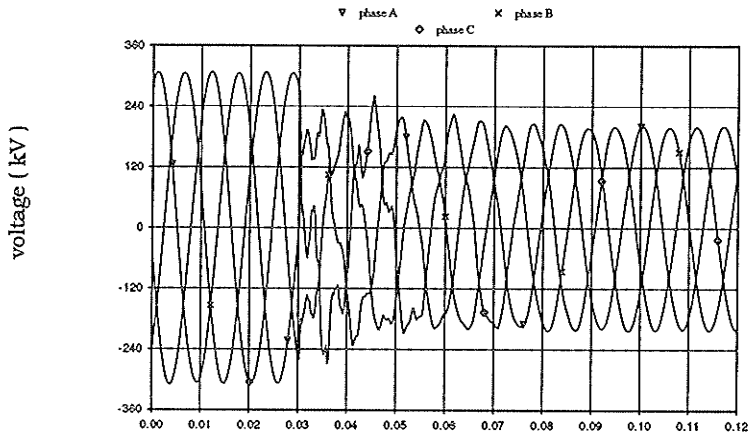

three phase to ground fault voltage

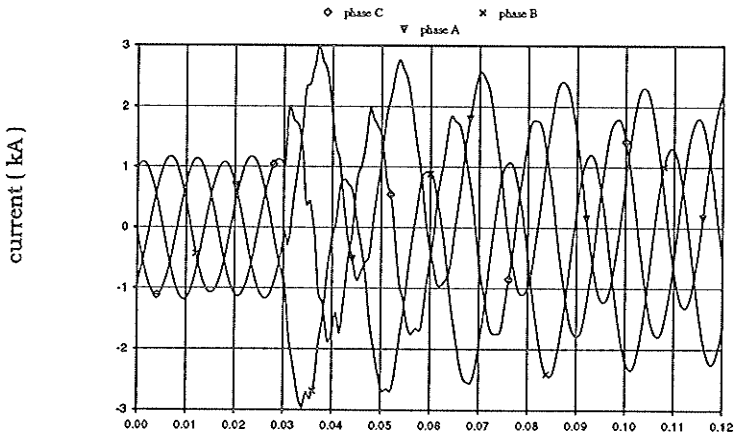

three phase to ground fault current

Figure 2 .3 : The current and voltage waveforms at location 6

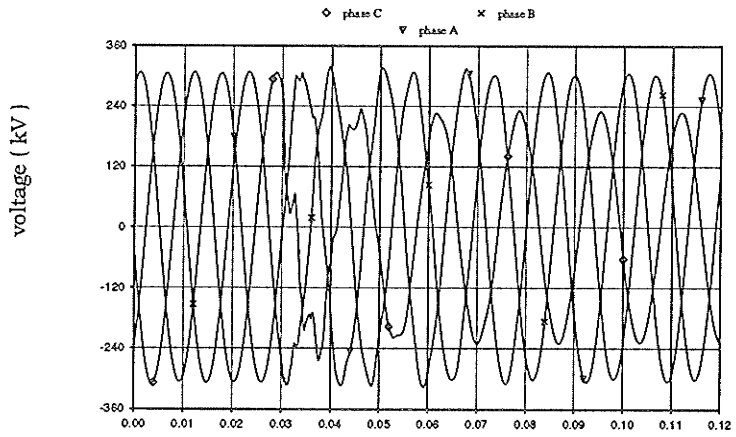

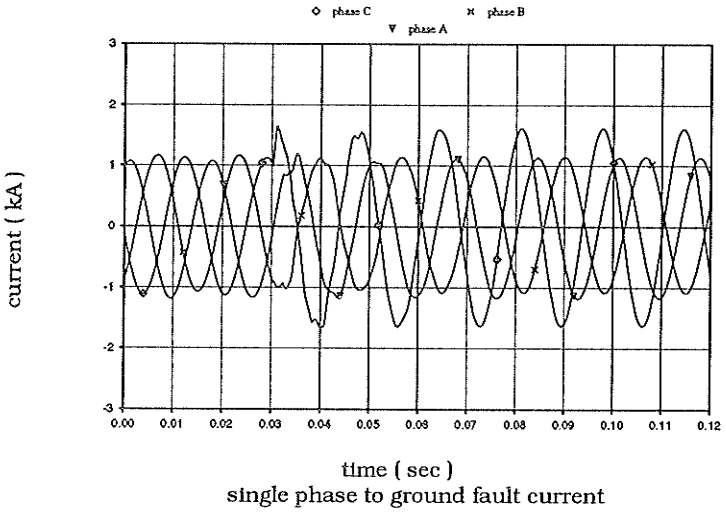

Figure 2 .4 : The current and voltage waveform at location 6

Our first case is to look at a three phase to ground fault at location 5 which is about 191 km away from the relaying point. The top two figures in Fig 2.5 are the voltage and current signals before and after the fault. The fault happens at 10 ms. The two figures at the bottom shows the result of the change of the impedance by the short window impedance measurement algorithm.

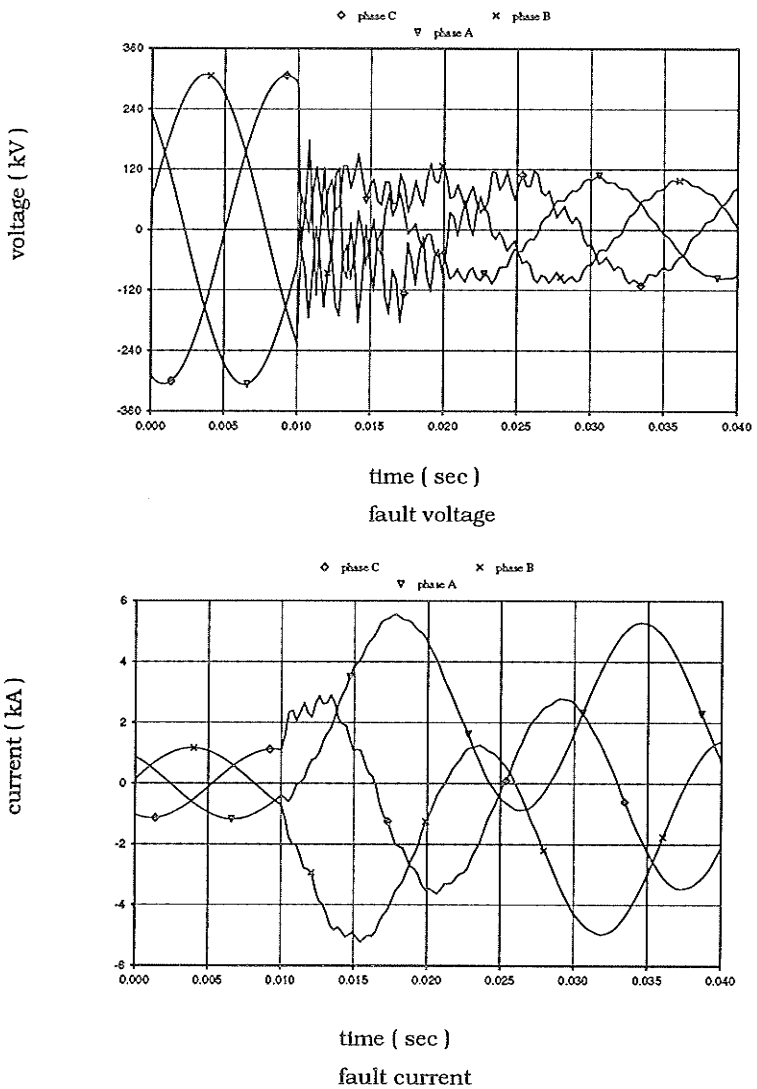

Figure 2 .5 : Fault voltage and current at location 5 for three phase to ground fault

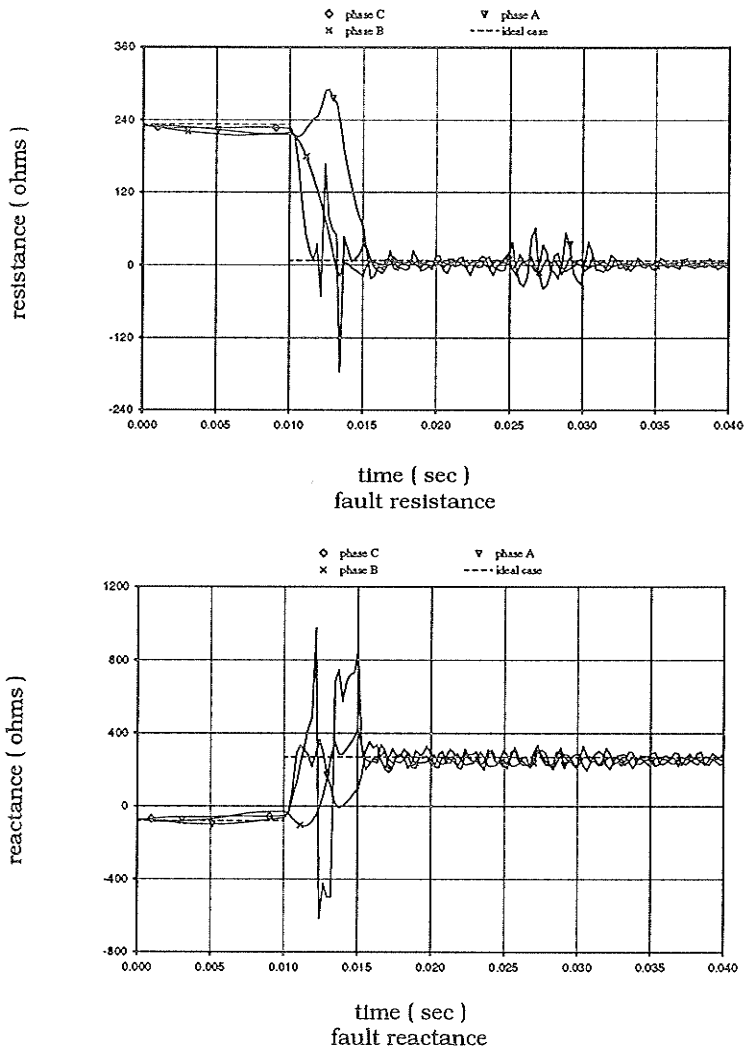

Figure 2 .6 : Measured resistance and retactance at location 5

Then we examine another fault situation at the same location for comparison. The figures are displayed in such a way that we can see the corresponding parts of different signals on the same time axis.

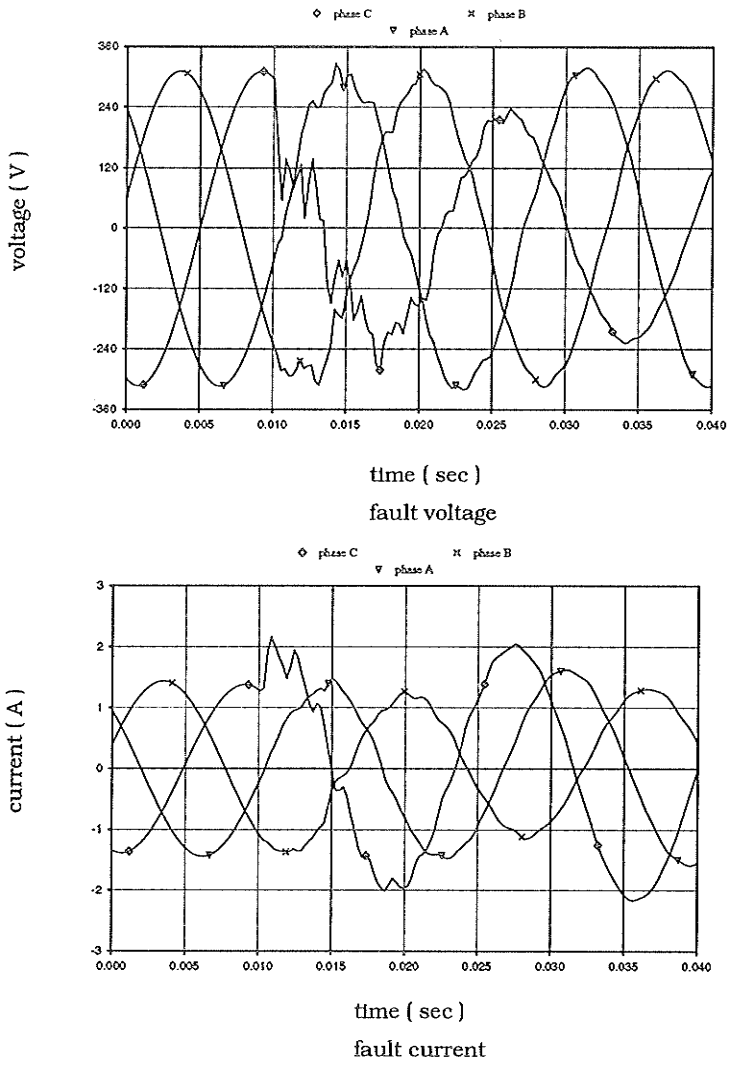

Figure 2 .7 : Fault voltage and current at location 5 for single phase to ground fault

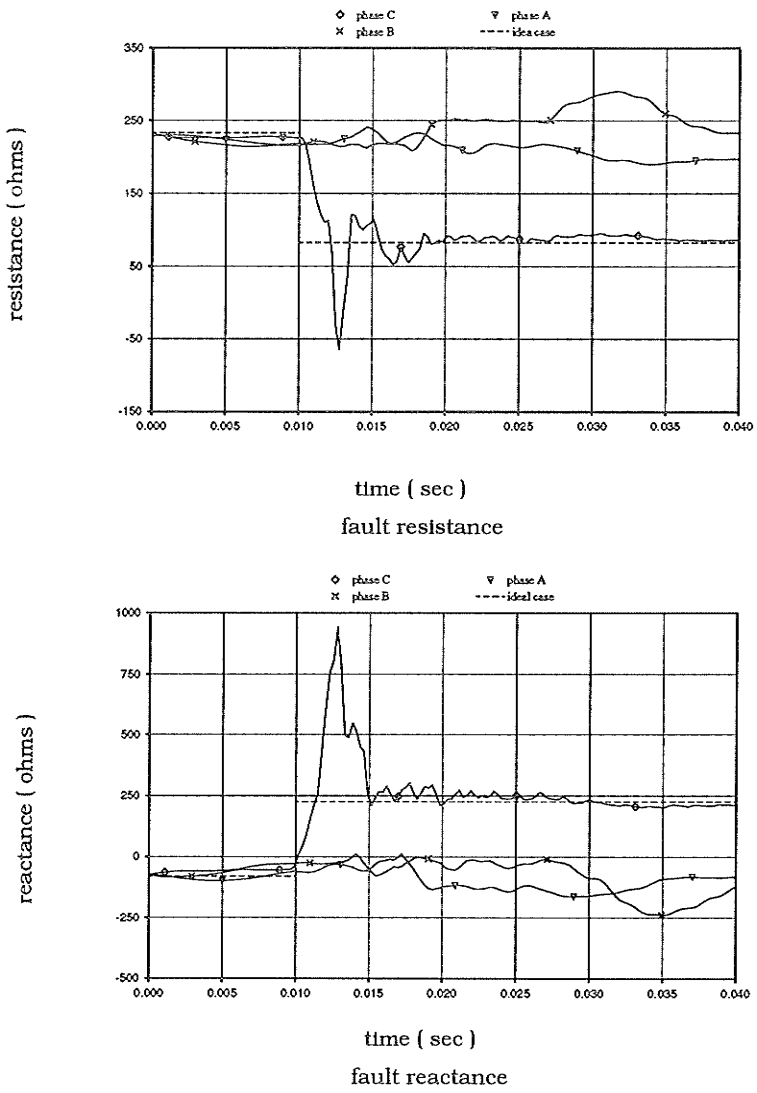

Figure 2 .8 : Measured resistance and reactance at locaiton 5

We can clearly see after the fault happens, that the system resistance will drop while the reactance will increase and the power transmission line system will change from the pre–fault steady state to fault steady state after a short while of transients. In the case of a three phase to ground fault the resistances in three phase will all drop down to about 20 ohm while the reactances increase to about 280 ohm. In the case of a single phase to ground fault, the resistance drops to about 80 ohm and the reactance increases to about 240 ohm only in the faulted phase, in the other phases the resistance and reactance will stabilize at the original

value after a while of transients caused by the coupling between the phases. In both cases, the transition periods are short (about 10 ms), and we can expect the response of the algorithm will be fast enough for reliable operation.

One thing that interests us is how good the algorithm will be when the fault happens at some remote location far away from the relay. Figure 2.9 illustrates the change in resistance and reactance after a single phase to ground fault at location 10 which is about 300 km from Dorsey. We can see that the impedance still has the same features as we have seen in figure 2.7 for location 5 but that they are less attenuated. The transient phenomena become very serious and in some cases some oscillations become so obvious that even a healthy phase behaves like a fault is happening for the initial transient period.

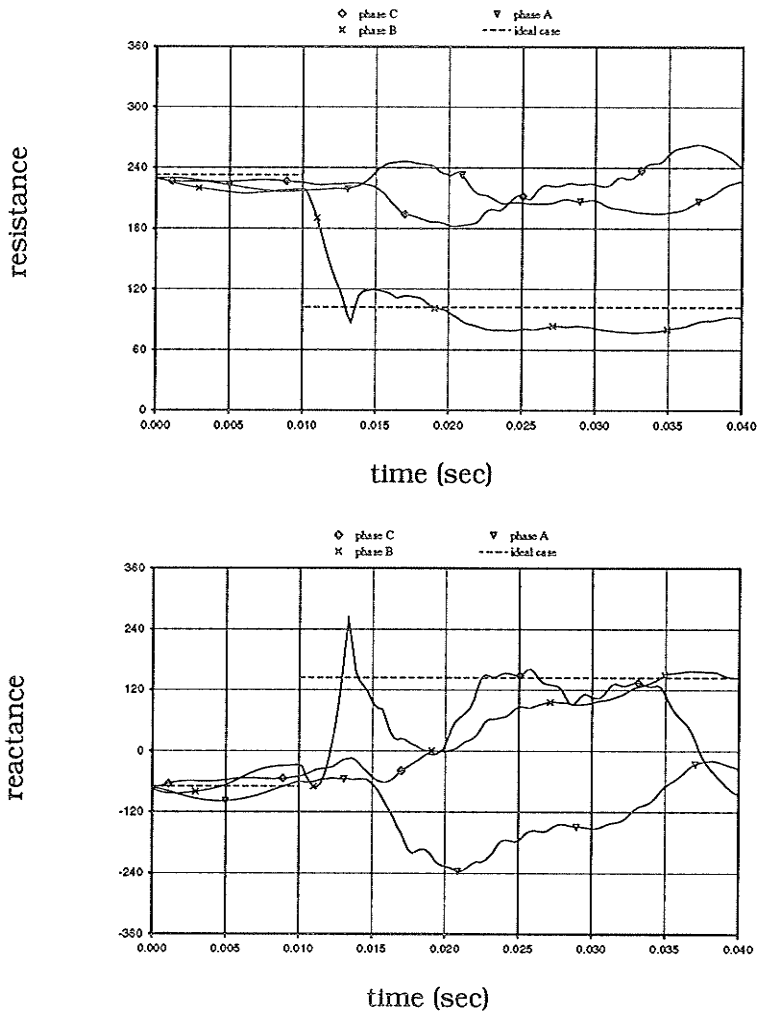

Figure 2 .9 : impedance measurement

The dynamic response of the technique can also be demonstrated by plotting the transient–impedance trajectory between the pre–fault and post–fault impedances.

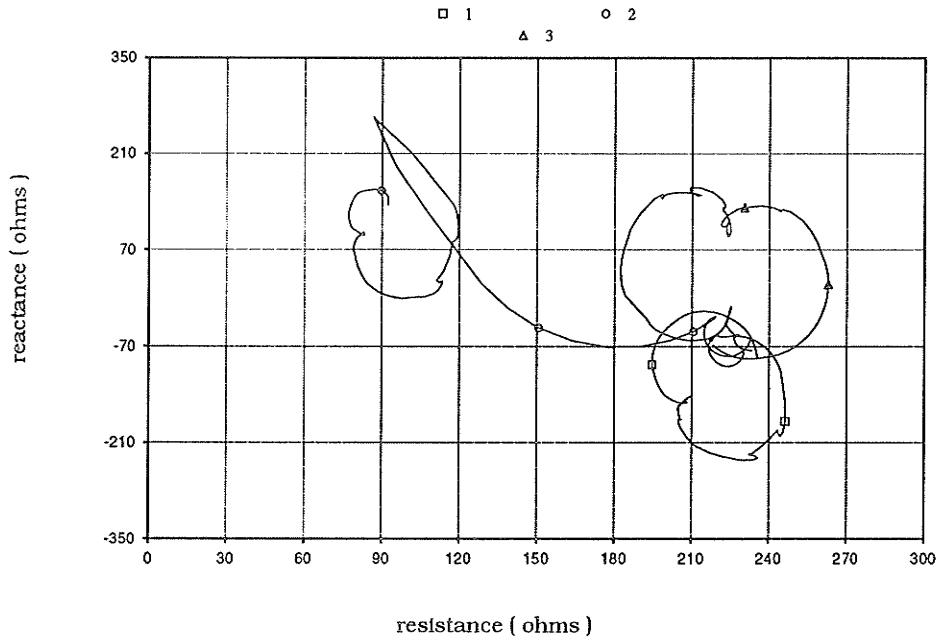

Figure 2 .10 : impedance trajectory for single phase to ground fault at location 10

Fig 2.10 shows the typical impedance trajectory of the result we obtained from the faulted waveforms at location 10. We can see from the graph that the original impedances for the three phases were centered at around 230 ohms for resistance and 80 ohms for reactance. At the inception of the fault the impedance begins to change dynamically. For two healthy phases the impedance trajectory loops around the central original impedance but in the faulted phase the impedance trajectory moves away from the original impedance, goes towards its new value and begins to loop around it.

Now we would like to make a comparison of three phase to ground fault happening at location 4 and location 7 which are 88 km and 444 km away from the relaying point, respectively. The resistance and impedances we obtained from both cases can be illustrated in figure 2.11 and figure 2.12.

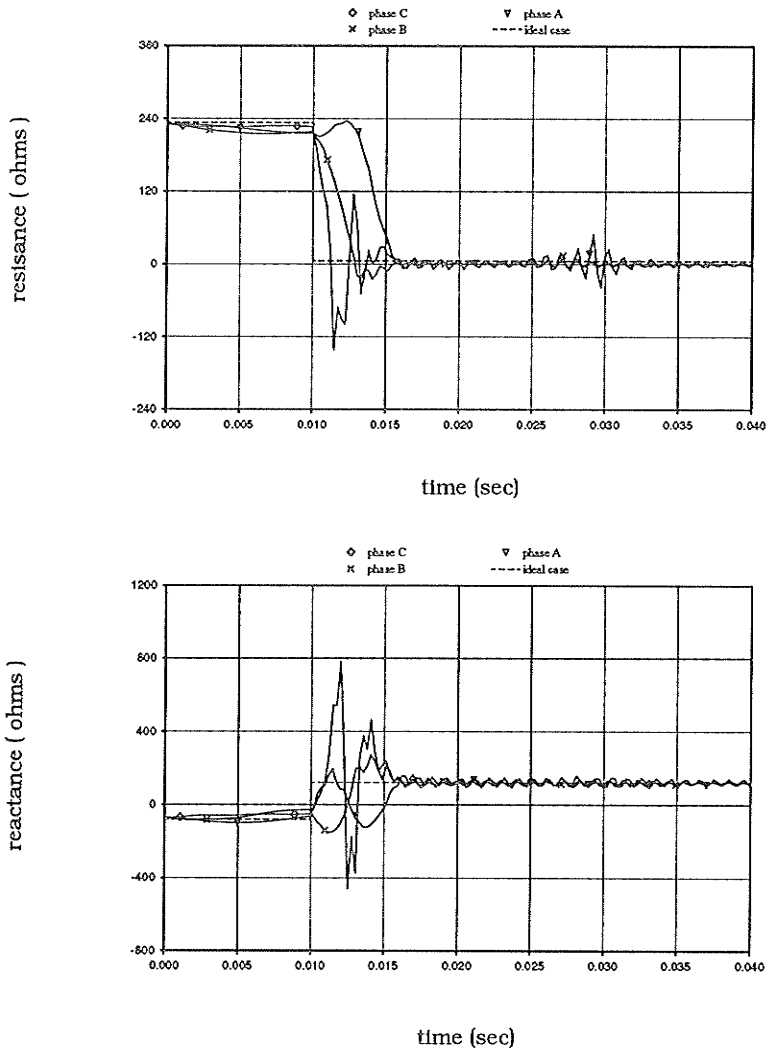

Figure 2 .11 : location 4 resistance and reactance after fault inception

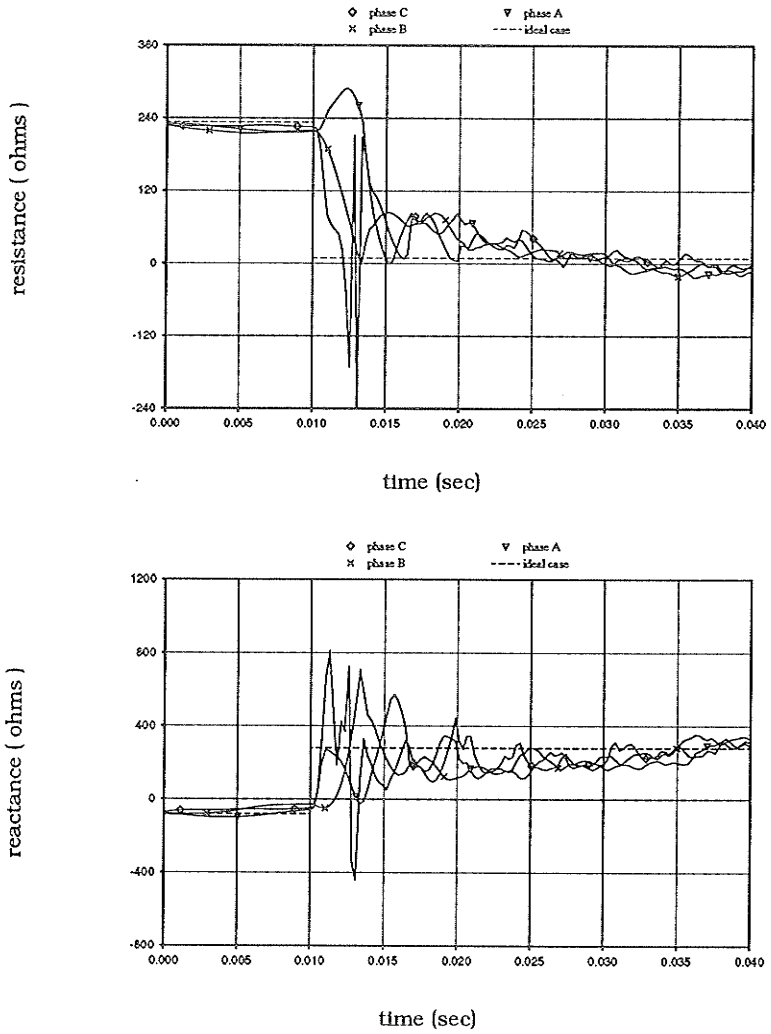

Figure 2 .12 : resistance and reactance after the fault inception at location 7

These figures further confirm the influence of distributed parameters towards the result of our computation using the fourier transform. At location 4, we can see the resistances and reactance converge to its steady state value within 10 ms after the fault inception for a very short period of transients. At location 7 which is 444 km away, the resistance and reactance we obtained from the fourier algorithm takes a lot more time to converge. By comparing the results, the impedance converges much more quickly and more attenuated at the location 4 than location 7.

2.4 PROBLEM AREAS AND LIMITATIONS

The impedance measurement algorithm using the fourier transform gives considerable rejection of non–fundamental components in the time available. The algorithm itself is rather straight forward and does not require the use of special high fidelity transducers.

The simulation results show that despite the fact that this algorithm gives an excellent response to the sudden change in the waveform, it suffers from the deterioration caused by dc offset, harmonics, and other high frequencies. The short window technique uses samples of less than 1 cycle and will certainly enhance the usual speed of about a cycle, but it is more susceptible to noise arising from features of the line which are not present in the lumped parameter model, that is, the travelling waves. Furthermore the concept of a power frequency impedance is not directly applicable to the period when the window contains both pre– and post–fault data.

If the fault happens at locations which are far away from the relaying point, the distributed capacitance makes the original R–L model no longer appropriate. This effect results in the vulnerability of the fourier impedance measurement algorithm in long distance cases. Thus some more effective methods of protection against faults at relatively long distances is required in order to ensure the correct operation of the device, or to reinforce the information that is already available.

Chapter 3
Travelling Wave Algorithm

3.1 INTRODUCTION

Travelling waves and surge phenomena in power systems are of importance in solving problems relating to protection of very long lines, fault location, switching of unloaded lines and calculation of recovery voltages on circuit–breakers under short–line fault conditions.

A significant advance in the solution of such problems was made by Fallou [20], who, with an assumption of complete symmetry of the conductors, applied the concept of symmetrical components to the solution of travelling wave phenomena. This method is limited, however, in that it yields average values for surge impedances and propagation coefficients, and this unfortunately masks important effects produced by asymmetry of conductors.

In this chapter a distance protection algorithm based on travelling wave information is briefly described. The algorithm first outlined by Crossley and Mclaren [1] uses the

distance relaying approach to detect a fault inside the protection zone. It has essentially two modules, the first detects the direction of the fault sensed at the relay station and the second determines the distance from the relay station to the fault when the fault is in the forward direction. A correlation technique was proposed to recognize the returning wave from the fault. A computer simulation based on this travelling wave distance protection algorithm is performed using the voltage and current signals generated by the EMTDC program. The results are analyzed in terms of different locations and different fault inception angles on the transmission lines.

It is necessary to start by introducing the concept of travelling wave in a single conductor transmission modal. The arrangement of a single conductor in the presence of an infinite earth plane is shown schematically in Figure 3 .1 .

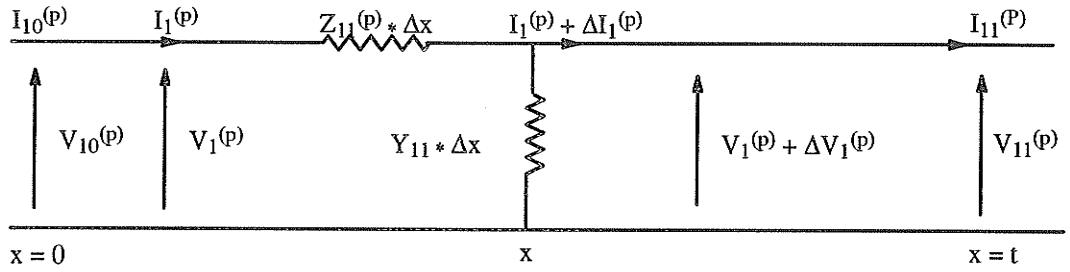

Figure 3 .1 : Equivalent circuit of single conductor system

The wave equation of a single phase, lossless line at a time t and point x on the line can be expressed as follows

$$-\frac{\partial e\ (x,\ t\ )}{\partial x} = l\frac{\partial i\ (x,\ t\ )}{\partial t}$$

$$-\frac{\partial i\ (x,\ t\ )}{\partial x} = c\frac{\partial e\ (x,\ t\ )}{\partial t} \qquad (3.1)$$

This equation establishes the relationship between the voltage and current at a certain time and a certain point on the line. The solution of these two equations produces two independent second order differential equations involving voltage and current :

$$-\frac{\partial^2 e(x,t)}{\partial x^2} = l\,c\,\frac{\partial^2 e(x,t)}{\partial t^2}$$

$$-\frac{\partial^2 i(x,t)}{\partial x^2} = c\,l\,\frac{\partial^2 i(x,t)}{\partial t^2} \qquad (3.2)$$

where l and c are the series inductance and shunt capacitance per unit length of the line. A general solution of the wave equations was first given by d'Alembert. This solution for equations (3.2) can be expressed by the following two equations:

$$e(x,t) = f_1(x-ut) + f_2(x+ut)$$

$$i(x,t) = \frac{1}{Z_0}\left\{f_1(x-ut) + f_2(x+ut)\right\} \qquad (3.3)$$

where Z_0 is the line characteristic impedance and u represents the line propagation velocity which corresponds to the velocity of electromagnetic waves in the ambient medium. Thus, the voltage and current at any time and any position along the line can be viewed as the superposition of two waves travelling in opposite directions.

A little mathematical manipulation gives us the following equations:

$$2f_1(x-ut) = V + IZ$$

$$2f_2(x+ut) = V - IZ \qquad (3.4)$$

where f1 and f2 are voltage waves passing through a measuring point x at time t. V and I are the measured voltage and current at the same point and at the same time. Substitute the time variables and we get the backward and forward relaying signals S1 and S2

$$S1(t) = 2f_2(t) = V(t) - Z_0 I(t)$$

$$S2(t) = 2f_1(t) = V(t) + Z_0 I(t) \qquad (3.5)$$

The occurrence of the fault is equivalent to the injection of a voltage at the point of fault, equal and opposite to the pre–fault steady state fault point voltage. Thus the so called

superimposed signals become very important for the travelling wave algorithms. The superimposed signals are obtained by subtracting the non–fault portion which is considered the same as the pre–fault signal one cycle ago from the faulted signal.

$$\Delta V(t) = V(t)_{post\text{-}fault} - V(t)_{pre\text{-}fault}$$
$$\Delta I(t) = I(t)_{post\text{-}fault} - I(t)_{pre\text{-}fault} \qquad (3.6)$$

The equation 3.5 can now be rewritten by using superimposed signals as:

$$S1(t) = \Delta V(t) - Z_0 \Delta I(t)$$
$$S2(t) = \Delta V(t) + Z_0 \Delta I(t) \qquad (3.7)$$

The incremental voltage and current phase signals are decoupled into three independent modes using the Karrenbauer Transformation.

$$\begin{bmatrix} V_p \end{bmatrix} = \begin{bmatrix} 1 & 1 & 1 \\ 1 & -2 & 1 \\ 1 & 1 & -2 \end{bmatrix} \begin{bmatrix} V_m \end{bmatrix} \qquad (3.8)$$

Applying the above equation to three phase voltage and current signals, we can get the superimposed voltages and currents. The values are further decoupled into mode values using the Karrenbauer Transformation.

Figure 3.2 shows the various voltage and current signals used to locate the fault. It shows single–phase–to–ground fault voltage and current waveforms. (the first row in fig 3.2) This signal will be processed to get the superimposed value by subtracting the pre–fault value. (the second row in fig 3.2). Then the superimposed value will be multiplied by the Karrenbaurer transformation matrix to get the corresponding modal superimposed current and voltage which become our subject to work with. (the third row in fig 3.2)

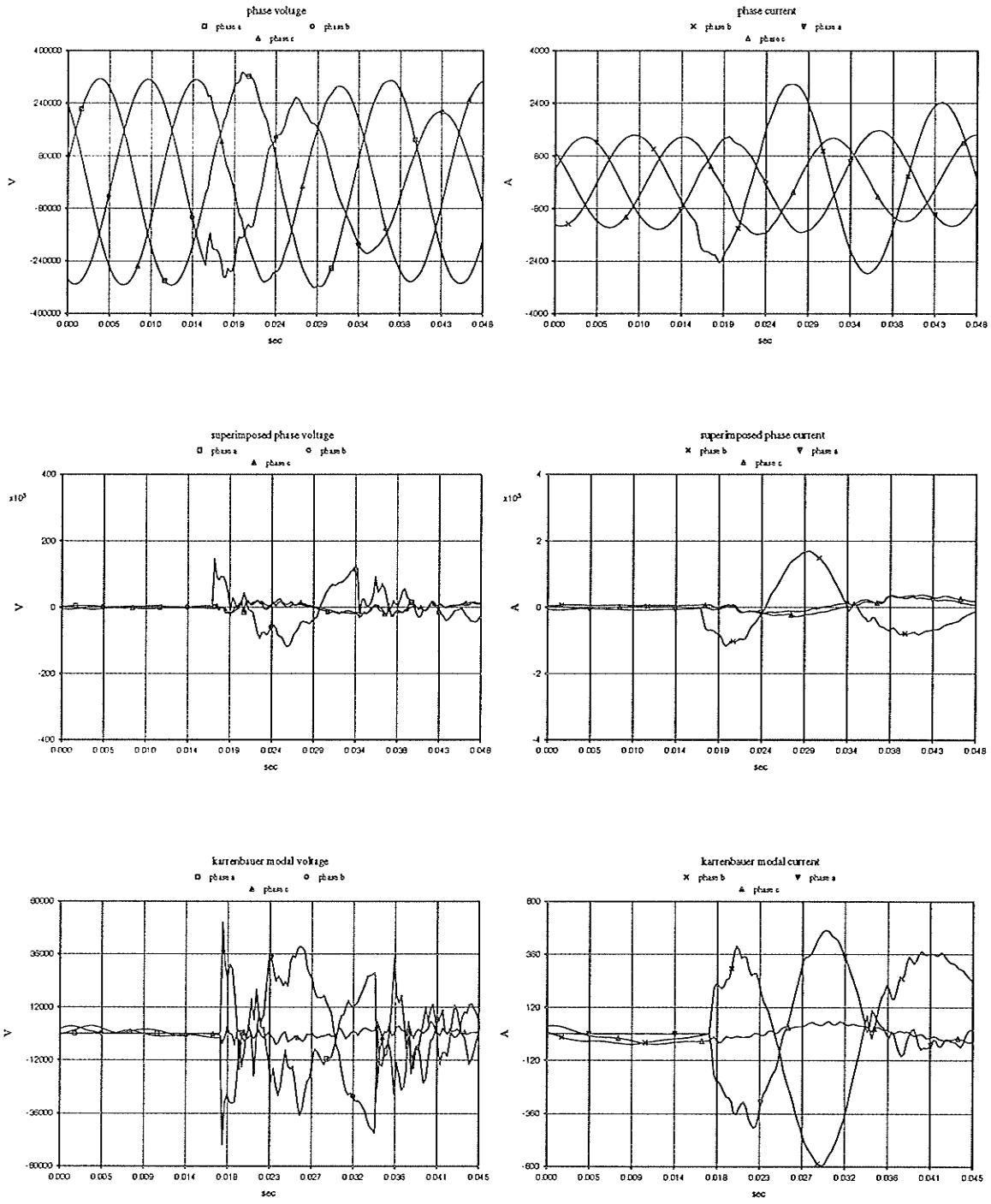

Figure 3 .2 : voltage and current signals used to locate the fault

It has been reported that this algorithm has some problems areas, particularly for single line to ground faults, such as reflection from the remote line end when interference with the reflection from the fault point causes mal–operation. The variation of the fault inception

angle affects the relaying signals and in turn the protection accuracy. Using a fixed correlation reference is not a valid representation of the wavefront for different fault types and positions. In addition, the close–up fault introduces another problem when no peaks corresponding to the fault location are found. All these problems limit the application of the proposed distance protection algorithm, although it is fast and accurate for faults involving two or more conductors since the fault appears as the total reflection point in front of the relay. In this chapter we discuss these problem areas in detail in order to develop some possible solutions.

It will be shown that the time delay between the initial forward wave, initiated by the fault, and entering the protection zone, and the associated reflected wave leaving the zone can be translated into the distance to the fault. The non–fault transients, the attenuation and distortion caused by other reflections and the frequency dependence of the transmission line parameters all interfere and may prevent true fault detection and location.

3.2 CORRELATION TECHNIQUE

The earth mode is frequency dependent, highly attenuated and has a slower velocity compared with the aerial modes. The distance obtained by using this mode was found to be inaccurate for faults occurring inside the protection zone. In this study, the aerial modes are examined since they give a more accurate result than the earth mode. The relaying signals for mode 2 in particular, are derived to process the protection technique. Mode 2 has a propagation velocity of 295km/ms and a modal surge impedance of 276 ohms. The relaying signals S1 and S2 describing the mode 2 propagation are rewritten once again:

$$S1_2 = \Delta V_{m2} - \Delta I_{m2} Z_{m2}$$

$$S2_2 = \Delta V_{m2} + \Delta I_{m2} Z_{m2} \qquad (3.9)$$

The fault location is determined by correlating a stored section of the S2 relaying signal describing the wave approaching the fault against sections of the corresponding S1 relaying signal describing wave returning from the fault. The delay which gives a cross–correlation maximum is multiplied by the corresponding propagation velocity to measure twice the distance between the relay and the fault. The S2 relaying signal illustrated graphically is multiplied by –1. This is extended to the cross–correlation in order to produce a positive peak corresponding to the fault location instead of a negative peak if the correlation performed between S1 and S2 is described by equations(5.13) and (5.14). Therefore S2 can be rewritten as:

$$S2_2 = -\left[\Delta V_{m2} + \Delta I_{m2} Z_{m2} \right] \qquad (3.10)$$

The distance algorithm described by Crossley and Mclaren uses a discrete cross–correlation of samples of the forward travelling wave function S2 with samples of the backward travelling wave function S1 in order to obtain the distance to the fault and avoid mal–operation. The discrete cross–correlation measures the degree to which sections of sampled signals X correlate with the delayed signal Y, that is , it measures the similarity of the two signals as a function of the delay

$$\phi_{xy}(t) = \frac{1}{N} \sum_{k=0}^{k=N-1} x(k+t) y(k) \qquad (3.11)$$

The practical implementation of the cross–correlation technique requires that a section of the forward travelling wave function, S2 to be stored. This section should represent the initial wavefront in the S2 relaying signal. To ensure the best representation of the wavefront, the stored section should include some samples recorded before the disturbance and some samples recorded after the disturbance. The manner in which this cross–correlation is done is as follows: the stored section of the backward travelling wave function S1 is constantly

being refreshed with the latest data. Cross–correlation is performed repeatedly as each new version replaces the existing one.

$$\phi_{s1,s2}(m\Delta t) = \frac{1}{N}\sum_{k=1}^{k=N} S1(k\Delta t + m\Delta t)S2(k\Delta t) \qquad (3.12)$$

where k = 1,2,... N and m= 0,1, . . . ∞ .

Also, mΔt is the delay between the sections, N is the number of the sample in every section and k is the sequence number of every particular sample in its corresponding section.

The cross–correlation function has a maximum when the section of the backward travelling wave signal S1 resembles the stored section of the forward wave signal S2. The difference in time between the arrival of the first disturbance in S2 and the peak of the cross–correlation function is then a measure of the total travel time corresponding to twice the distance to the fault.

The sections of the relaying signals S1 and S2 have different mean levels on which the travelling wave components are superimposed. When the discrete cross–correlation function is applied to such signals, the different mean levels prevent a meaningful correlation between the stored section of S2 signal and the S1 signal. To avoid this problem the correlation is performed between sections from which the section mean levels have been removed. The elements of these new sections are defined as follows,

$$S1_R(k\Delta t + m\Delta t) = S1(k\Delta t + m\Delta t) - \frac{1}{N}\sum_{k=1}^{k=N} S1(k\Delta t + m\Delta t)$$

$$S2_R(k\Delta t) = S2(k\Delta t) - \frac{1}{N}\sum_{k=1}^{k=N} S2(k\Delta t) \qquad (3.13)$$

The cross–correlation between sections of S1 and S2 with zero mean can be defined as:

$$\phi_{s1,s2}(m\Delta t) = \frac{1}{N}\sum_{k=1}^{k=N} S1(k\Delta t + m\Delta t)S2(k\Delta t) \qquad (3.14)$$

Maximum output of the correlation function indicates the best match between the wave–shapes. The time delay, $m_{max}\Delta t$, when this occurs can be used to determine the distance to the fault:

$$x_f = m_{\max}\Delta t\frac{u}{2} \qquad (3.15)$$

where u is the velocity of the mode being considered.

The cross–correlation fault locator commences its operation after the direction detector indicates a forward fault. A forward fault decision occurs when the S2 signal exceeds a pre–determined threshold after the S1 signal has exceeded the threshold. The length of the stored section of S2 relaying signal depends mainly upon the fault position and is proportional to the mode propagation velocity. To ensure that the cross–correlation reference contains a section of the S2 signal describing the initial wave approaching the fault, the stored section contains samples included both before and after the direction decision.

3.3 PROTECTION SIMULATION

A computer simulation of the distance protection algorithm is used to process the voltage and current signals generated by the power system program in order to determine the fault location. The protection simulation provides an ideal implementation of the protection technique described in the preceding section. The simulation is ideal because it analyses the discrete numerical data exactly as expressed in the equations describing the protection algorithm without the distortion or noise associated with the hardware. The voltage and current signals generated by the simulation are calculated at a rate of 64 samples per 60 Hz cycle.

The power system program is used to calculate the post–fault actual voltage and current signals for one power–frequency cycle duration. The incremental voltage and current signals are derived by subtracting the pre–fault steady state voltage and current signals from the corresponding post–fault signals.

These signals are monitored at the relay station located at Dorsey. To start the correlation process, a section of the S2 signal representing the wavefront is stored. The duration of this section of S2 signal should include some samples before and some samples after the fault disturbance to ensure the best representation of the wavefront. Before the correlation process takes place, the mean values of the stored section of the S2 signal and the S1 section are removed.

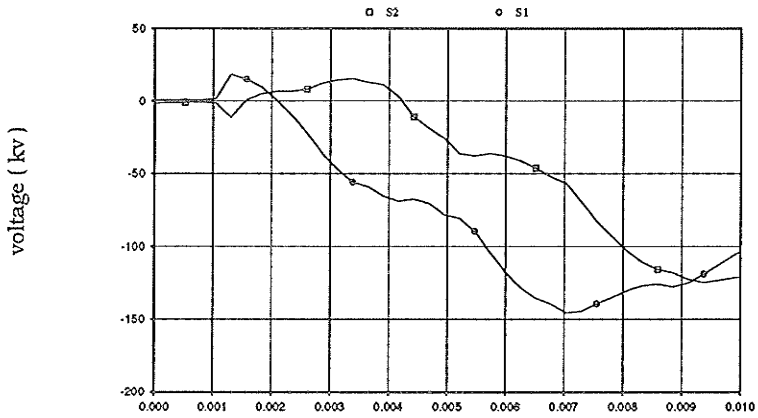

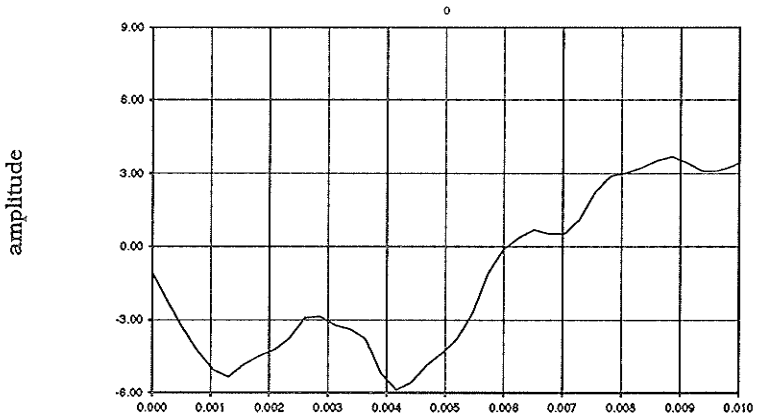

Figure 3 .3 three phase to ground fault at location 6

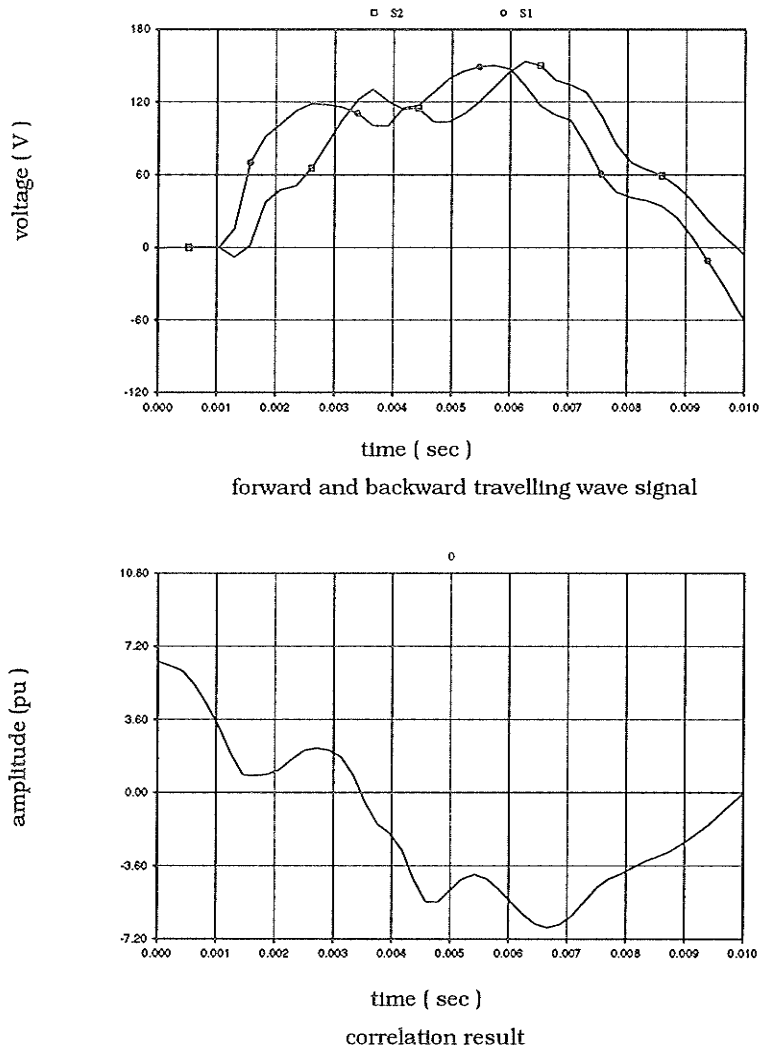

Figure 3 .4 : single phase to ground fault at location 6

In order to examine the validity of this distance measurement algorithm, the relaying signals and the protection responses for two different fault types are illustrated in figure 3.3 and figure 3.4. The faults are a three line to ground fault and a single line to ground fault respectively. The faults occur at location 6 which is about 330 km from the relay, on the given system configuration.

Comparing the protection response for different faults will help in examining the advantages and limitations of the technique as a distance protection. The correlator output for the three line to ground fault indicates a time delay for a well defined peak at time delay

of 2.5 ms which gives a 750 km distance to the fault. The result indicated for the single line to ground fault gives a delay time to the first peak of 2.5 ms corresponding to a distance of 375 km. This result roughly matches the available fault information.

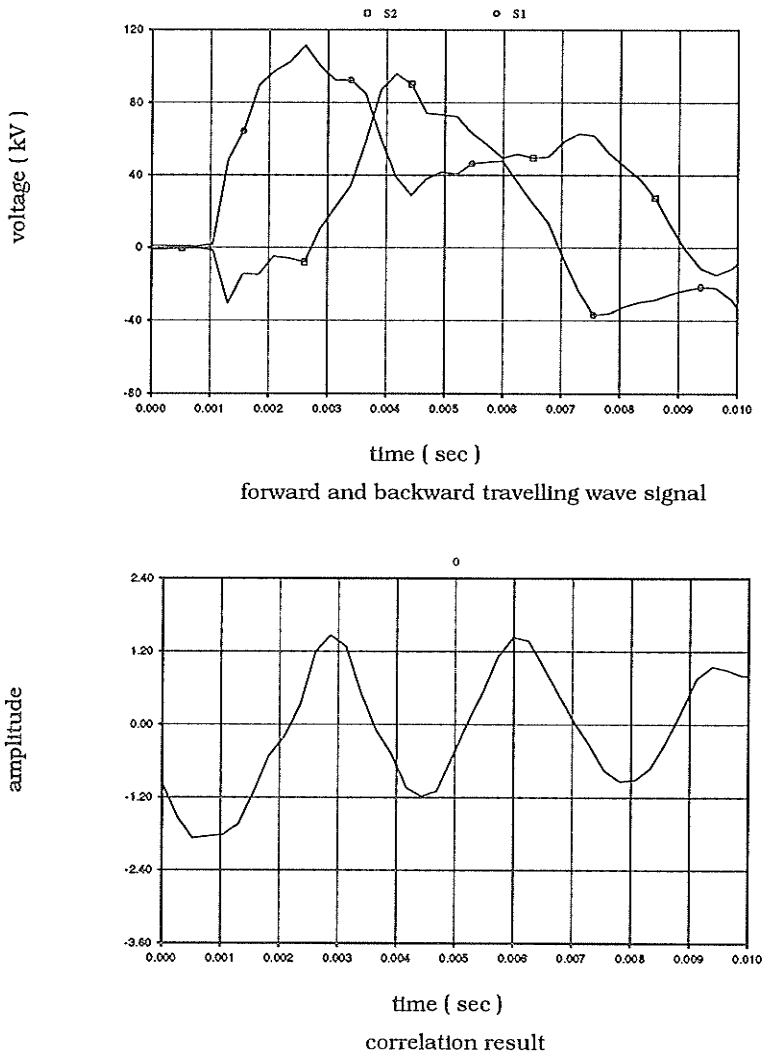

Figure 3 .5 : Single phase to ground fault at location 7

Fig 3.5 shows the correlator response at location 7 which is 444 km away from the relaying station. We notice that in this situation, the position of the peak moves back a little as a result of the increase in the distance to fault from the relaying station. We can see the

first peak is at about 3.0 ms which corresponds to 450 km in distance to the fault . This is about the position for location 7 where the fault happens.

The magnitude of the high frequency transient initiated by a fault is dependent on the fault inception angle on the phase voltage wave. This means that the magnitude of the travelling wave on the relaying signals initiated by a fault is dependent on the fault inception angle. The relaying signals for a fault occurring at or near the zero crossing on the voltage wave become very small in magnitude and have a slow rate of rise relative to those for a fault occurring at 90 degrees. As a result, the stored section of S2 signals used in the fault location process may not describe the initial wavefront, so the cross–correlation function and the distance to the fault will not be valid.

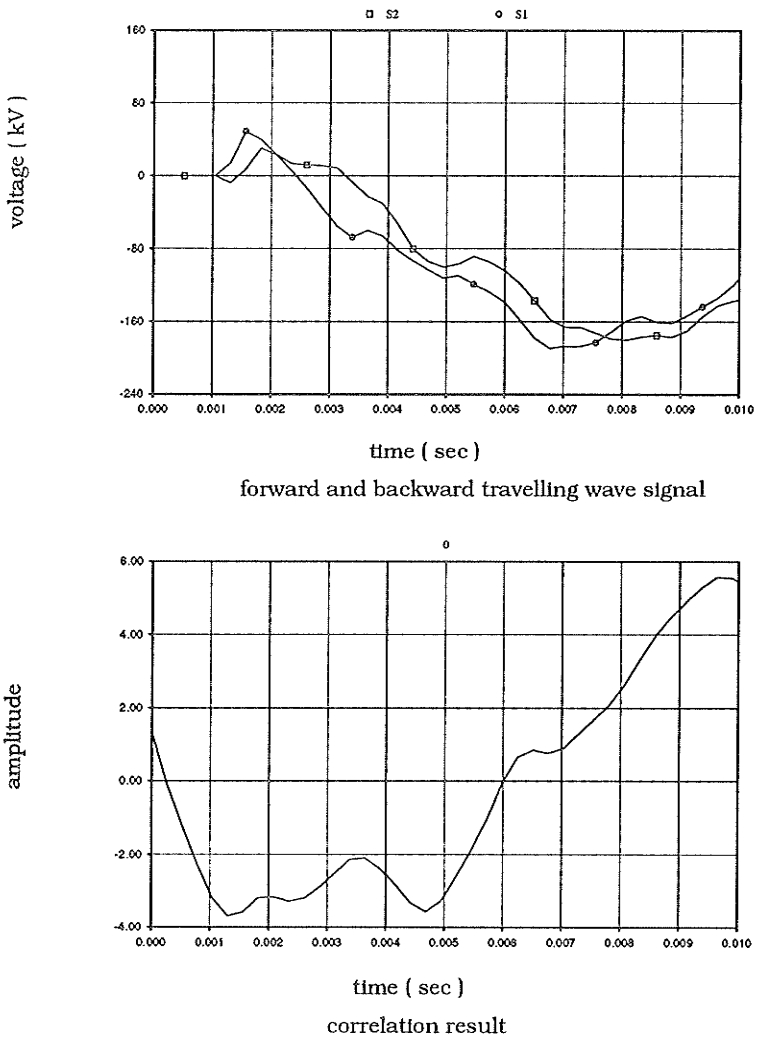

Figure 3 .6 : Single phase to ground fault at inception angle near 0 at location 9

Fig 3.6 shows a single phase to ground fault at location 9 which is about 260 kms away from the relaying point. The relaying signal magnitude is small and has a slow rate of rise, particularly in the first few milliseconds as is shown in the left figure. The correlator output magnitude in such a situation will increase as a ramp function similar to the S1 signal. The correlator output is shown at the right. The first peak gives the correct distance to the fault but has a magnitude less than that of the successive peaks representing the other reflections from the fault. This can be explained if we refer to the relaying signals in figure 3.6. The stored section of the S2 relaying signal is correlated with sections of the S1 signal

representing the waves returning from the fault point. These waves are similar in shape to the stored section because the fault is considered as a total reflection point, but the slope of successive wavefronts increases and the correlator output for successive wavefronts thus increases. Therefore the peaks corresponding to the 2nd and the 3rd wavefronts returning from the fault have magnitude larger than that of the first peak. A well–defined peak at 2.0 ms corresponding to a fault distance of 300 km from the relay is indicated by the correlator output, for faults near the remote end, mal–operation is expected. Faults involving two conductors sometimes also give rise to such problems.

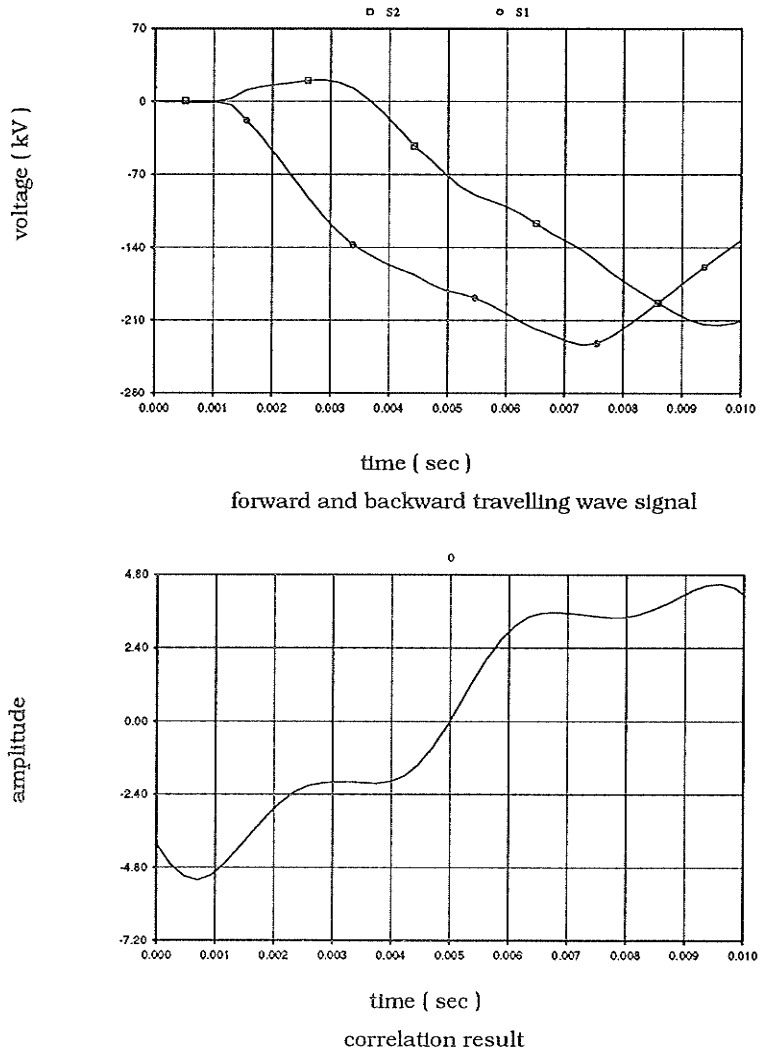

Figure 3 .7 : phase to phase fault at inception angle 0 at location 6

Figure 3.7 shows the relaying signals and the correlator output for the double line to ground fault. The fault inception angle of phase A is zero degrees and the fault occurs at location 6 which is about 330 km from the relay. The reflection from the fault point is clearly evident in the relay signals. The correlator output indicates peaks at 2.5 ms corresponding to the twice the distance from the fault.

In general, fault inception angle near or at zero crossing reduces the protection accuracy and the protection reach for single line to ground faults. This is particularly true in the case of a fault which occurs at the remote end of the protection zone when the frequencies and amplitude of the travelling waves are low.

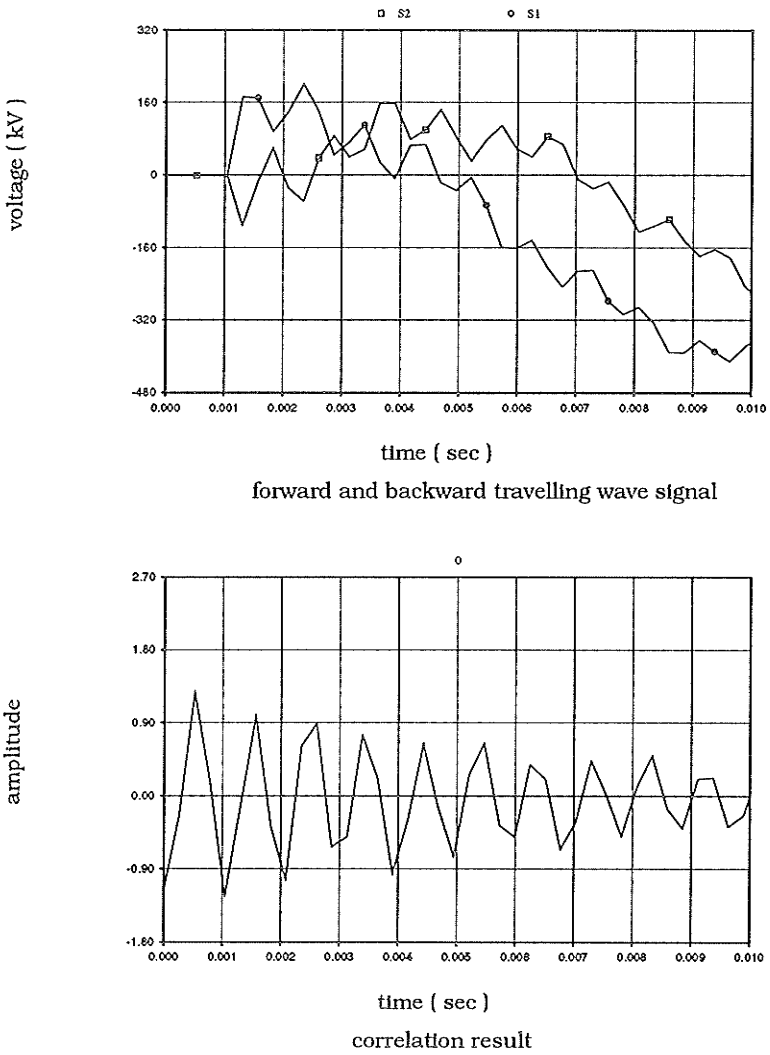

Figure 3 .8 : Close up three phase to ground fault at location 4

Fig 3.8 shows the relaying signals and the protection response for a close–up fault. The fault occurs at location 4 which is 88 km from the relay located at busbar 1. The successive reflections from the fault appear very clearly on the relaying signals for a duration of 0.5 ms and the relaying signals follow the basic frequency of the faulted phase voltage thereafter. A stored section duration greater than 0.5 ms will fail to recognize the first reflection wave returning from the fault point. The 0.5 ms roughly corresponds to a distance of 75 km, which is about 17% off the location of the fault.

3.4 PROBLEM AREAS AND LIMITATIONS OF THE ALGORITHM

In order to examine the original distance protection algorithm based on travelling waves, the current and voltage signals are generated by simulating the power system under fault conditions. The phase signals are decomposed into three independent modes by using modal analysis theory. The features of the forward and backward relaying signals have been discussed and the results indicate that these signals could be used as the basis for an integrated relay with multiple functions such as directional discrimination,fault location, fault classification and phase selection.

The distance protection algorithm based on the travelling waves provides a number of significant advantages but not without some limitations. The travelling waves initiated by a fault depend not only on the fault position but also on the fault type, the fault inception angle and the power system configuration. Such factors as these will consequently have an influence on the decision made by the relay. The effect of the fault position, resistance and inception angle upon the frequency and the magnitude of the high frequency transients will appear directly on the first wave initiated by the fault. After this wave has been reflected at the discontinuity point behind the relay, the reflection coefficient will introduce a new factor affecting the magnitude and shape of the forward wave travelling towards the fault point.The distance to the fault is measured by observing the return of the initial forward wave to the relaying station after being reflected at the fault location.

In general, the correlation technique has some distinct advantages over the impedance measurement algorithm in that it responds faster because we are using the high frequency travelling waves. It has established itself as a major protection scheme in long line applications. The only limitation is the case when the fault happens at the inception angle close to or at the zero crossing point. Some other schemes have to be introduced to tackle the problem.

Chapter 4
Wavefronts Prediction Algorithm

4.1 INTRODUCTION

It has already been established that the travelling wave protection technique is the fastest way in the transmission line protection. In order to estimate the fault position this technique uses the rapid change of the wavefront, i.e. the superimposed current and voltage signals, to correlate its reflection.Then the position of the peak value of the correlator indicates the two–way travelling time between the test and fault points. Despite the fact that this technique may handle most situations, especially as we know faults almost always occur closer to the 90^0 of POW, when fault occasionally occur at or near 0^0 of POW where there is no rapid change at the wavefront, correlation technique may not give a good result.

In this chapter, a new theory of wavefront prediction is described. This algorithm makes use of the voltage and current measurement at the sending end to predict a fault wavefront occurring in multiconductor transmission lines under the condition that the type of fault is clearly known. Then this information is used to estimate the fault distance.

As we all know, upon fault inception two components of travelling wave are generated, one in the forward direction the other in the backward direction. As shown in Fig.4.1 the propagation of the fault wave is rather messy at the later stage due to the multi–reflections. The proposed wavefront prediction technique is only valid in the initial period before other reflecting waves reached the relay point. The wavefront herein is restricted in the sense of strictly at the initial period of the fault inception without considering multi–action generated by the fault.

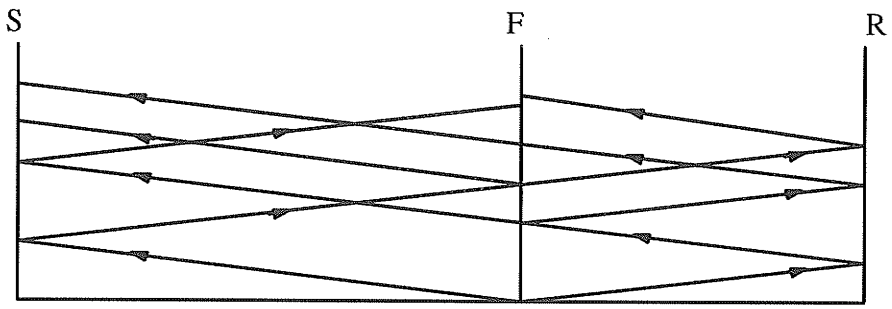

Figure 4 .1 : Propagation of the fault wavefront as a result of multi–reflections

4 .2 MODAL EXPRESSION OF THE FAULT CONDITION

For a multiconductor transmission line, in order to decouple the mutual effects between lines, modal transformation can be used to transform the n+1 conductor line system into an n independent modal line system . After modal transformation, in a three–phase transmission line system, a phase to ground fault may not be a short circuit in the corresponding modal line system. As a result, it is necessary to take a closer look at modal representation of different fault conditions.

In a three phase line configuration, the fault condition can be expressed by the following Y–matrix at the fault position

$$Y_p = \begin{bmatrix} y_{aa} & y_{ab} & y_{ac} \\ y_{ba} & y_{bb} & y_{bc} \\ y_{ca} & y_{cb} & y_{cc} \end{bmatrix}$$

(4 .1)

where y_{aa}, y_{ba}, .. etc. are the fault admittance between phases or between phase and ground.

For instance, for a phase A to ground fault, it is

$$Y_p = \begin{bmatrix} y_a & 0 & 0 \\ 0 & 0 & 0 \\ 0 & 0 & 0 \end{bmatrix}$$

(4 .2)

where y_a is the fault admittance between the phase and ground.

For a phase A to phase B fault, it is

$$Y_p = \begin{bmatrix} y_{ab} & -y_{ab} & 0 \\ -y_{ab} & y_{ab} & 0 \\ 0 & 0 & 0 \end{bmatrix}$$

(4 .3)

where y_{ab} is the fault admittance between the two phases.

The corresponding modal voltage and modal current matrix are obtained by multiplying the phase voltage and current by the inverse of a modal transformation matrix, namely, S :

$$V_m = S^{-1} V_p$$
$$I_m = S^{-1} I_p$$

(4 .4)

Accordingly, the fault modal admittance matrix can be expressed by

$$Y_m = S^{-1} Y_p S$$

(4 .5)

If the modal transformation matrix uses Karrenbauer transform, then

(4 .6)

$$S = \begin{bmatrix} 1 & 1 & 1 \\ 1 & -2 & 1 \\ 1 & 1 & -2 \end{bmatrix}$$

It's inverse matrix will be

$$S^{-1} = \frac{1}{3} \begin{bmatrix} 1 & 1 & 1 \\ 1 & -1 & 0 \\ 1 & 0 & -1 \end{bmatrix}$$

(4.7)

As an example, for the above phase A to ground fault, the corresponding modal admittance at the fault point is

$$Y_m = \frac{y_a}{3} \begin{bmatrix} 1 & 1 & 1 \\ 1 & 1 & 1 \\ 1 & 1 & 1 \end{bmatrix}$$

(4.8)

From this matrix we may find out that in the modal representation, a phase A to ground fault will affect all three modes and is no longer a single mode to ground fault.

For a phase B to ground fault, the corresponding Karrenbauer modal admittance is

$$Y_m = \frac{y_b}{3} \begin{bmatrix} 1 & -2 & 1 \\ -1 & 2 & -1 \\ 0 & 0 & 0 \end{bmatrix}$$

(4.9)

It is obvious that this matrix is different from the phase A to ground fault case in which the mode 2 is not affected.

For a phase A to phase B fault, the Karrenbauer modal admittance is

$$Y_m = 3y_{a_b} \begin{bmatrix} 0 & 0 & 0 \\ 0 & 2 & 0 \\ 0 & 1 & 0 \end{bmatrix}$$

(4.10)

We may find that for this kind of fault, the ground mode is not affected. The physical meaning is easy to imagine.

In the same manner, we can obtain the modal representation of the admittance in all types of fault situations and find that they are all different from each other. We will use this information at a later stage.

4.3 PHASE SELECTION ALGORITHM

Faulted phase selection, and hence selective pole tripping , is an important relaying capability because it increases the system stability as well as its availability. Fault classification is an indispensable part of the wavefront prediction scheme because prediction demands a priori knowledge about fault situations.

A slightly different approach is adopted for the modal transformation. We use the Clarke transform instead of the Karrenbauer transform because the former can discern more cases. The Clarke transform can be expressed as

$$V_p = \begin{bmatrix} 1 & 1 & 0 \\ 1 & -1/2 & \sqrt{3}/2 \\ 1 & -1/2 & -\sqrt{3}/2 \end{bmatrix} V_m \qquad (4.11)$$

o r its inverse

$$V_m = \frac{1}{3} \begin{bmatrix} 1 & 1 & 1 \\ 2 & -1 & -1 \\ \sqrt{3} & 0 & -\sqrt{3} \end{bmatrix} V_p \qquad (4.12)$$

Subtracting the corresponding value from one cycle (64 samples) ago, we can get the superimposed modal signals.

The discriminants for fault detection in a three phase line are defined by utilizing the superimposed modal voltages and currents at the relaying point as follows

$$D_F^{(k)} = (\Delta v_R^{(k)} - Z^{(k)} \Delta i_R^{(k)})^2 + \frac{1}{\omega^2} \left[\frac{d}{d\tau} (\Delta v_R^{(k)} - Z^{(k)} \Delta i_R^{(k)}) \right]^2 \qquad (4.13)$$

for the forward discriminant and

$$D_B^{(k)} = (\Delta v_R^{(k)} + Z^{(k)} \Delta i_R^{(k)})^2 + \frac{1}{\omega^2} \left[\frac{d}{d\tau} (\Delta v_R^{(k)} + Z^{(k)} \Delta i_R^{(k)}) \right]^2 \qquad (4.14)$$

for the mode (k) backward discriminant, where $Z^{(k)}$ is the mode (k) surge impedance, and $\Delta v_R^{(k)}$ and $\Delta i_R^{(k)}$ are the mode (k) superimposed voltage and current respectively at relay point R. In discrete form, the forward discriminant equation becomes:

$$D_f^{(i)} [k] = (S1^{(i)} [k])^2 + \frac{N^2}{4 \pi^2} \left\{ S1^{(i)} [k] - S1^{(i)} [k - 1] \right\}^2 \qquad (4.15)$$

where $$S1^{(i)} [k] = (\Delta V^{(i)} [k] - Z^{(i)} \Delta I^{(i)} [k]) \qquad (4.16)$$

and the differential term can be found by subtracting S1 signal at k instant by itself one sample instant ago.

In real practice, the above equation is further simplified because the phase selecting scheme is based entirely upon the truth table of the discriminants, what concerns us is the binary value of the disciminants, i.e whether it is above a threshold or below it.

The new forward discriminant equation is :

$$D [k] = | S1 [k] | + \frac{1}{4} \left| \frac{S1' [k]}{\omega} \right| \quad \text{for} \quad | S1 [k] | > \left| \frac{S1' [k]}{\omega} \right| \qquad (4.17)$$

or

$$D [k] = \frac{1}{4} | S1 [k] | + \left| \frac{S1' [k]}{\omega} \right| \quad \text{for} \quad | S1 [k] | < \left| \frac{S1' [k]}{\omega} \right| \qquad (4.18)$$

The accuracy of this approximation is acceptable, because of the binary nature of the algorithm. The main advantage of this discriminant function is the independence of the fault initiation angle and the possibility of combining the different modal components to achieve faulted phase selection and fault classification.

If we change the base phase to b and to c , we get all disciminant values corresponding to each phase. A threshold value is used to change the discriminants into binary numbers:

$D_f = 1$ when D_f > threshold

$D_f = 0$ when D_f < threshold

Now, we just look at the truth table of the Clarke transform

FAULT		L – G			L – L			L – L – G			3L – G
Basis	D_f	a	b	c	a–b	b–c	c–a	a–b	b–c	c–a	
Ph " a "	D^0	1	1	1	0	0	0	1	1	1	0
	D^1	1	1	1	1	0	1	1	1	1	1
	D^2	0	1	1	1	1	1	1	1	1	1
Ph " b "	D^0	1	1	1	0	0	0	1	1	1	0
	D^1	1	1	1	1	1	0	1	1	1	1
	D^2	1	0	1	1	1	1	1	1	1	1
Ph " c "	D^0	1	1	1	0	0	0	1	1	1	0
	D^1	1	1	1	0	1	1	1	1	1	1
	D^2	1	1	0	1	1	1	1	1	1	1

Table 4 .1 : Truth Table for Clarke Transform

We can use a small subroutine to search among the truth table to get the fault type

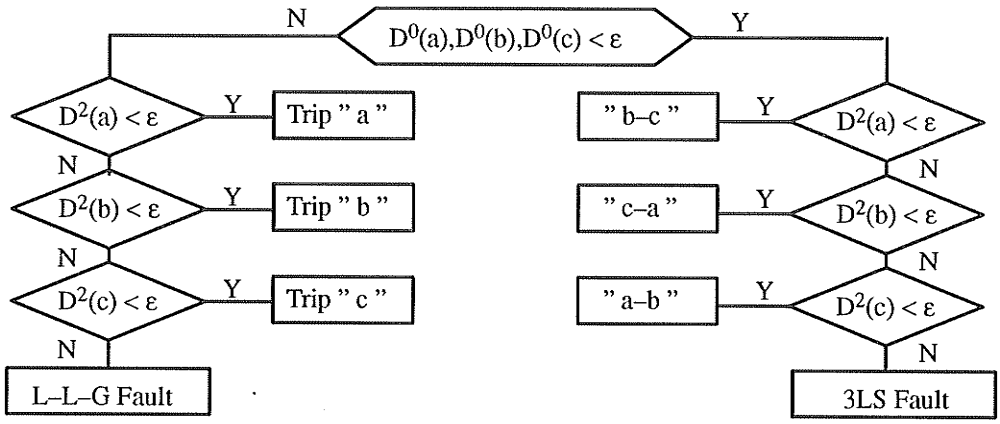

Figure 4 .2 : flowchart diagram for discriminant algorithm

thus by comparing with the truth table, we will be able to know exactly what type of fault is involved. Also, we find out the base phase that we can use later in the algorithm.

4 .4 PREDICTION OF THE WAVEFRONT

In order to predict the fault wavefront we use the fact that any disturbance induced in the line system spreads in the form of travelling wave. So, before the disturbance's arrival, the state of any point keeps its stationary condition.

Now we have to switch back to the Karrenbauer Transform because it performs better in the travelling wave situation

$$[V_p] = \begin{bmatrix} 1 & 1 & 1 \\ 1 & -2 & 1 \\ 1 & 1 & -2 \end{bmatrix} [V_m] \qquad (4.19)$$

For modal admittance matrix

$$[Y_m] = \begin{bmatrix} 1 & 1 & 1 \\ 1 & -2 & 1 \\ 1 & 1 & -2 \end{bmatrix}^{-1} [Y_p] \begin{bmatrix} 1 & 1 & 1 \\ 1 & -2 & 1 \\ 1 & 1 & 2 \end{bmatrix} \qquad (4.20)$$

Using modal transformation and referring to the system in fig 4.3, in the pre–fault condition we can calculate the modal incident wave and reflection wave by means of the phase voltages and currents of the sending end S.

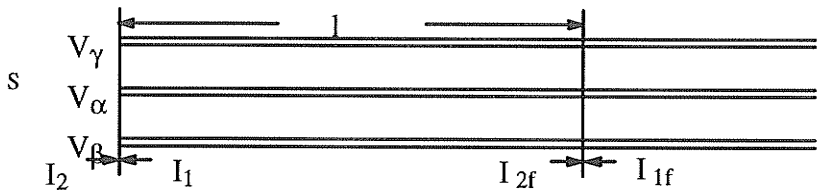

Figure 4 .3 : Three phase transmission line

The corresponding modal incidental current matrices I_1 and the reflection current I_2 at the sending end are

$$I_1(t) = I_s(t) - Y_0 V_s(t)$$
$$I_2(t) = -I_s(t) - Y_0 V_s(t) \qquad (4.21)$$

If the distance between sending end and the fault point is l, then the incident and reflection currents at the fault point F are

$$I_{1f}(t) = I_1\left(t + \frac{l}{v}\right) = I_1(t + \tau)$$
$$I_{2f}(t) = I_2\left(t - \frac{l}{v}\right) = I_2(t - \tau) \qquad (4.22)$$

where v is the speed of the travelling wave of the corresponding mode, and t is wave travelling time along line l .

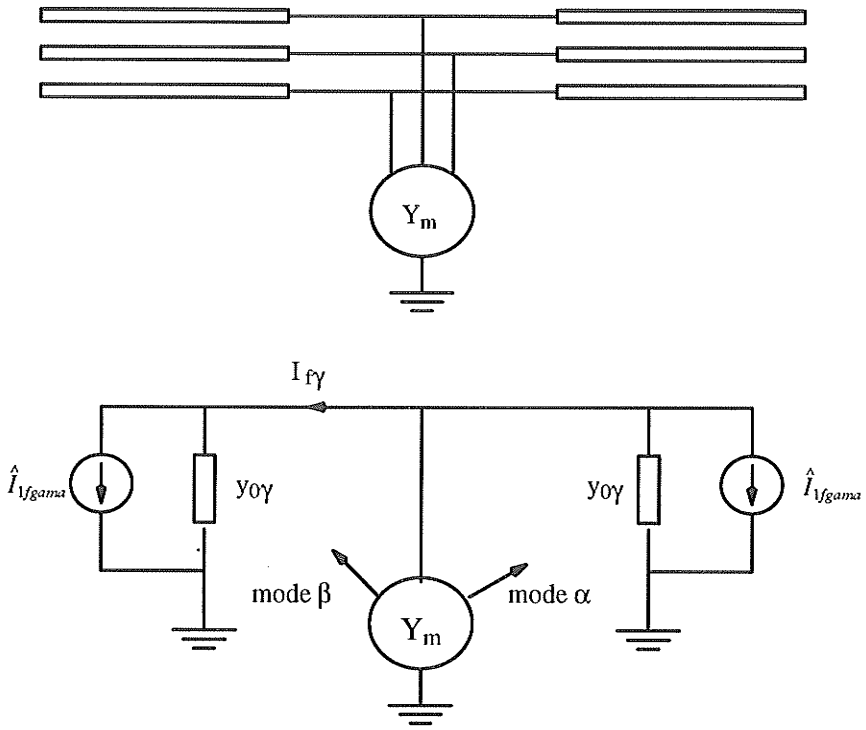

Figure 4 .4 : system model under fault conditions

If the fault inception time is t0 , at time t0+ the situation can be depicted by Fig 4.4. where Y_m is the fault admittance matrix,. Then the network Y_m is excited by the current sources I_{1f} (t0+) and I_{2f} (t0+) which can be considered as the stored energy in the form of travelling waves just arriving at point F form both directions.

The following equation can be readily established

$$- I_{1f} (t) - I_{2f} (t) = Y_{mm} V_f (t) \qquad (4 .23)$$

where

$$Y_{mm} = 2 Y_0 + Y_m = 2 \begin{bmatrix} y_{0\gamma} & 0 & 0 \\ 0 & y_{0\alpha} & 0 \\ 0 & 0 & y_{0\beta} \end{bmatrix} + Y_m \qquad (4 .24)$$

$y_{0\gamma}$,, $y_{0\alpha}$ and $y_{0\beta}$ are the surge admittances for the 3 modes, and Y_m is the fault admittance matrix. Equation 4.23 can be rewritten as

$$V_f(t) = -Y_{mn}^{-1}\left\{\hat{I}_{1f}(t) + \hat{I}_{2f}(t)\right\} \tag{4.25}$$

The incident current at the sending end is

$$I_1(t+\tau) = I_f(t) + Y_0 V_f(t) \tag{4.26}$$

It can be further expressed by all the values measured at the sending end only, as

$$I_1(t+\tau) = -\hat{I}_2(t+\tau) + 2\,Y_0\,Y_{mn}^{-1}\left\{\hat{I}_1(t+\tau) + \hat{I}_2(t-\tau)\right\} \tag{4.27}$$

All the values with a hat sign indicate that they are the prediction values of the corresponding signals.

Subtracting both sides of the above equation by the predicting value of I_1 which is based on the measurement of pre–fault state, we get

$$I_1(t+\tau) - \hat{I}_1(t+\tau) = -\hat{I}_1(t+\tau) - \hat{I}_2(t+\tau) + 2\,Y_0\,Y_{mn}^{-1}\left\{\hat{I}_1(t+\tau) + \hat{I}_2(t-\tau)\right\}$$

If we define

$$S_1(t+\tau) = I_1(t+\tau) - \hat{I}_1(t+\tau)$$

which means the discrepancy of post–fault incidental current and pre–fault steady state incidental current and thus we get

$$S_1(t+\tau) = (2\,Y_0\,Y_{mn}^{-1} - I)\left\{\hat{I}_1(t+\tau) + \hat{I}_2(t-\tau)\right\} \tag{4.28}$$

where

$$A = 2\,Y_0\,Y_{mn}^{-1} - I \tag{4.29}$$

A is named as fault condition matrix. This equation gives the relation between the incident fault incremental signals and the pre–fault signals.

One more thing to notice is that we don't use the superimposed signals anymore, we use the actual measured values in this algorithm.

Reorganizing the algorithm we get

$$S_1(t+\tau) - A\,I_1(t+\tau) = A\,I_2(t-\tau) \qquad (4.30)$$

Notice that all the values with respect to the instant $t+\tau$ are on one side and all values with respect to instant $t-\tau$ are now on the other side. Two new signals $F_1(t)$ and $F_2(t)$ can be generated:

$$F_1(t) = S_1(t+\tau) - A\,I_1(t+\tau)$$

$$F_2(t) = A\,I_2(t-\tau) \qquad (4.31)$$

We know from equation 4.30 that

$$F_1(t+\tau) = F_2(t-\tau) \qquad (4.32)$$

The above equation is only valid for a short period before the secondary reflection occurs at the fault point.

Now we can easily construct F_1 and F_2 signals using all the information we have obtained so far. Comparing the phase shift between the two signals F_1 and F_2, we will be able to find the difference

$$d = |F_1(t_1) - F_2(t_2)| \qquad (4.33)$$

which is a constant over a period of time T_s. The T_s is the searching range which is determined by the protection zone of the line.

Then the distance to the fault can be determined as :

$$l = \frac{T_s\, v}{2} \qquad (4.34)$$

where v is the propagation speed of the phase which can be approximated as the speed of light.

A complete reference of F_1 and F_2 in terms of different fault situations can be found in the appendix.

As an example, for a phase A to ground fault:

$$Y_{mm} = 2\,Y_0 + Y_m = 2\begin{bmatrix} y_{0\gamma} & 0 & 0 \\ 0 & y_{0\alpha} & 0 \\ 0 & 0 & y_{0\beta} \end{bmatrix} + \frac{y_a}{3}\begin{bmatrix} 1 & 1 & 1 \\ 1 & 1 & 1 \\ 1 & 1 & 1 \end{bmatrix}$$

Note the last term is the phase A to ground modal admittance matrix

$$A = 2\,Y_0\,Y_{mm}^{-1} - I$$

If we substitute the inverse matrix of Y_{mm} into the above equation, we can obtain the fault condition matrix A. Usually the fault resistance is much smaller than the surge characteristic impedance of the modal line, y_α will be a big number compared with $y_{0\gamma}$, $y_{0\alpha}$, or $y_{0\beta}$. We can make the assumption A can be approximated as the limit of A when y_α goes to infinite:

$$\lim_{y_a \to \infty} A = \frac{-1}{a+b+c}\begin{bmatrix} a & b & c \\ a & b & c \\ a & b & c \end{bmatrix}$$

where

$$a = y_{0\alpha}\,y_{0\beta} \qquad b = y_{0\beta}\,y_{0\gamma} \qquad c = y_{0\gamma}\,y_{0\alpha}$$

If we plug these results into equation 4.31 and note in the steady state the ground mode components of the modal signals are equal to zero .

$$f_{1\alpha}(t) = S_{1\alpha}(t) + \frac{1}{a+b+c}\left[b\,\hat{I}_{1\alpha}(t) + c\,\hat{I}_{1\beta}(t) \right]$$

$$f_{2\alpha}(t) = -\frac{1}{a+b+c}\left[b\,\hat{I}_{2\alpha}(t) + c\,\hat{I}_{2\beta}(t) \right]$$

Comparing the $f_{1\alpha}$, $f_{2\alpha}$, we can find the distance to fault.

4.5 SIMULATION RESULT

A complete computer simulation is conducted using the proposed wavefront prediction technique. The transmission line data is obtained from the EMTDC simulation programme. The test is conducted at different locations along the transmission line. The fault types involves single phase to ground and double phase to ground faults and all happen at inception angle of zero degrees. All the result figures will show the f1 and f2 signal and their phase difference at the range where the difference is approximately a constant.

The line used for this study is the 500 kV line from Dorsey to Forbes and Chisago and has been shown in Fig1.3. There are 4 transposition points on the line which is 539 km overall. The test values are waveforms for voltages and currents at Dorsey. The simulation results of the phase to ground fault at location 9 are given in Fig 4.5 . The distance from the location 9 to the relay is roughly 260 km. The horizontal shift between the corresponding parts of curves f1 and f2 is 2τ as expected from eqn 4.32.

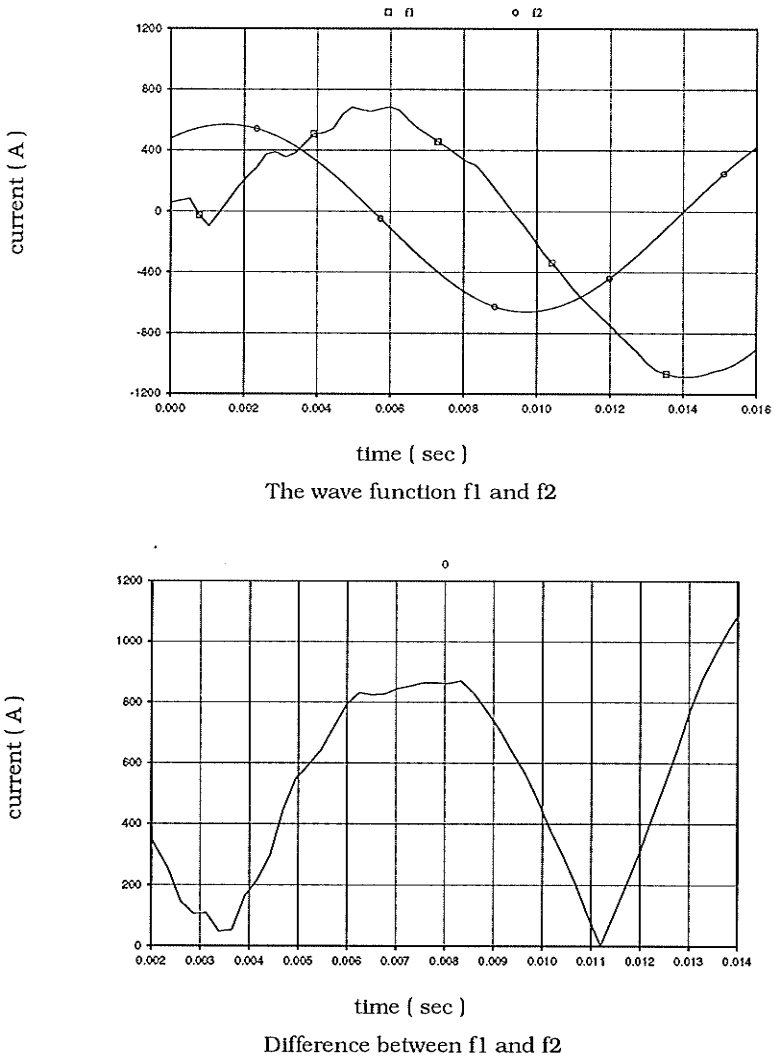

Figure 4 .5 : Single phase to ground fault at location 9

Fig 4.5 shows the single line to ground fault of 0 inception angle at location 9. From the fig. 4.5 we can clearly see that the initial part of f_2 (t) is approximately a sine wave of the same shape as f_1 (t). The time displacement of the two signals is shown the at the bottom figure. It shows the signal d= | f1 – f2 | as defined in Eqn 4.33. The difference function shows a period when d is relatively flat, approximately from the instant of 6.5 ms to 8.5 ms. This period is defined as T_s and theoretically can be defined as the period the derivitive of d is within a certain threshold. As we can see in the later cases that this definition sometimes will be confusing because when the difference is not that ideal, we just use the turning point

of the signal as the start and the end of T_s . The time for which T remains a constant for is about 2.5 ms which is roughly twice the travel time between the fault and the relay. This is a further reinforcement of the basic measurement for the travel time to and from the fault from Dorsey.

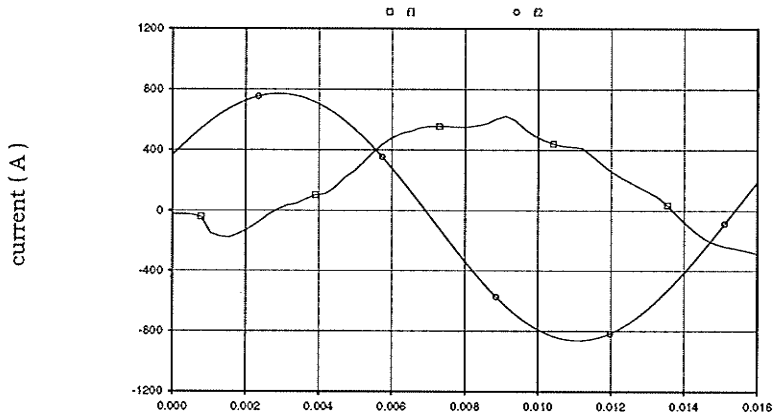

The wave function f1 and f2

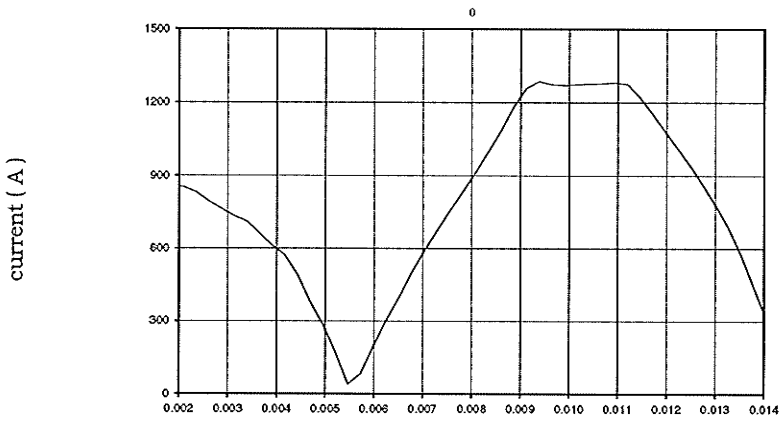

Difference between f1 and f2

Figure 4 .6 : single phase to ground fault at location 6

For a single phase to ground fault at location 6 as shown in fig 4.6, the wavefront predicting algorithm also gives a correct result. It shows a flat peak of about 2 ms which corresponds to twice the distance from the fault location (location 6) to the relay station.

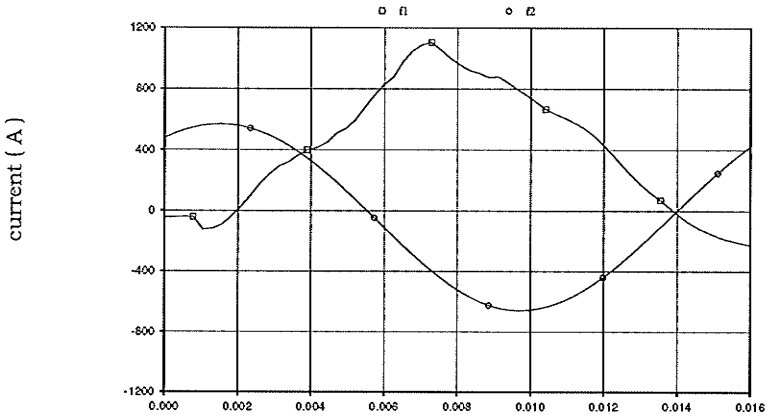

The wave function f1 and f2

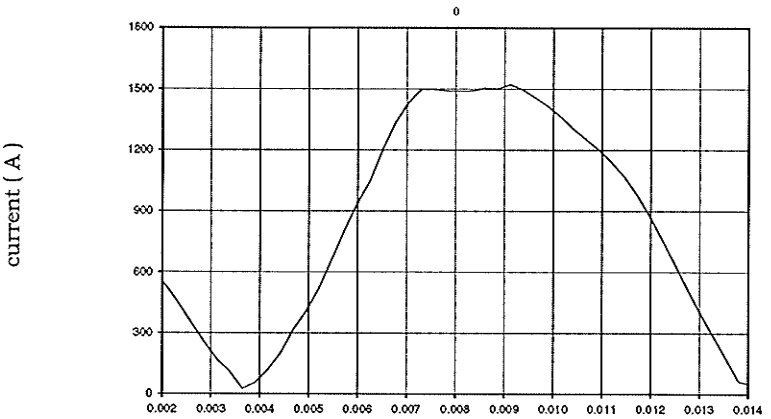

Difference between f1 and f2

Figure 4 .7 : f1 f2 signal for phase a to phase b fault at location 6

Fig 4.7 depicts a phase to phase fault at location 6. In the upper figure, the f1 signal looks slightly like f2 just after the turning point, and in the lower figure we can see the absolute value of the difference between the f1 and f2. It shows that the constant portion of

| f1 – f2 | is about 2.2 ms which corresponds to 646 km in distance . This matches what we know about location 6.

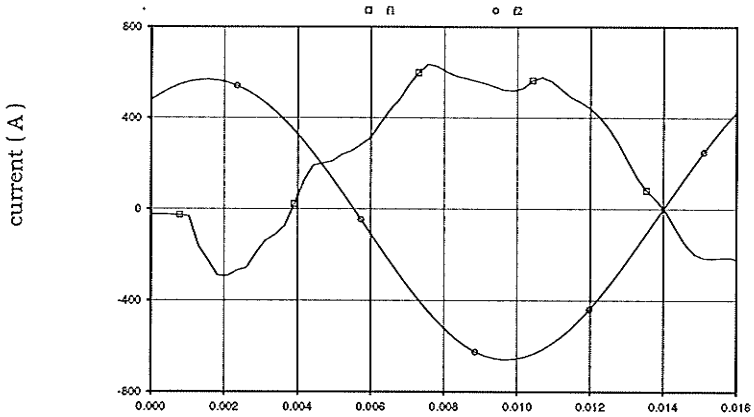

The wave function f1 and f2

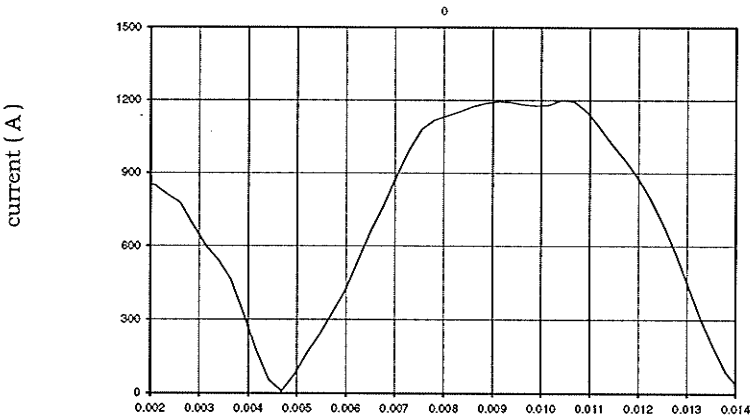

Difference between f1 and f2

Figure 4 .8 : single phase to ground fault at pow 0 degree at location 7

Fig 4.8 depicts the situation for a single phase to ground fault at location 7 which is about 450 km away from the relaying station. It is very interesting to see that the f1 signal even curves a little bit to match the f2 signal . The bottom figure shows that the constant part of difference between f1 and f2 lasts about 3 ms. This corresponds to twice the distance from the fault at location 7 to the relay station.

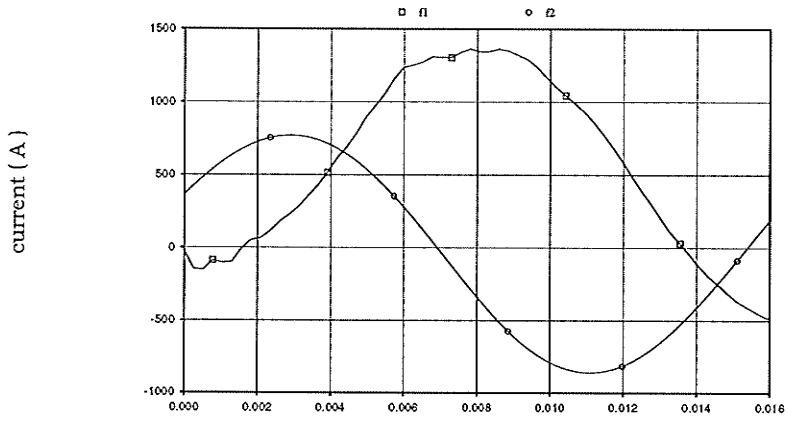

The wave function f1 and f2

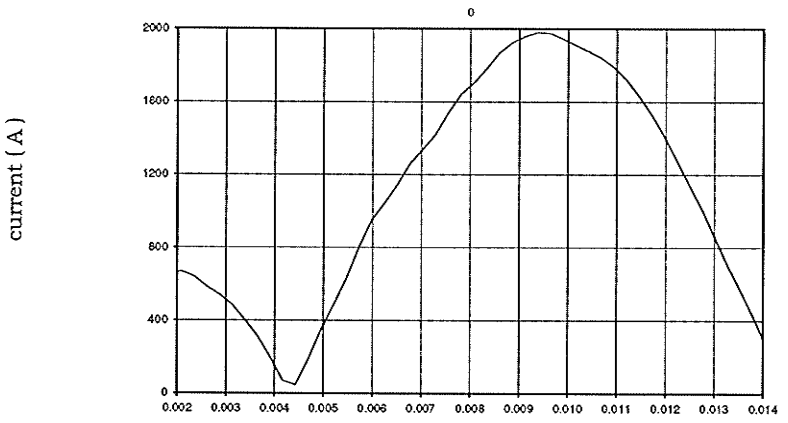

Difference between f1 and f2

Figure 4 .9 : single phase to ground fault at location 4

There are cases when even at 0^0 P.O.W the wavefront predicting algorithm will not work as in the situation shown in Figure 4.9. This is a close–up single phase to ground fault at location 4. From the bottom figure we can see that the algorithm fails to give a flat peak, this is because of the reflection from the close source which changes the shape of the wavefront after the fault.

4.6 PROBLEM AREAS AND LIMITATIONS

The wavefront algorithm is an effective method in support of the travelling wave correlation scheme. The fault wavefront in a multiconductor transmission line depends on the fault condition matrix, the pre–fault incident and reflection waves which can be measured at the sending end. At the fault point, not only reflection occurs but also mode mixing. The wavefront is more complicated than the situation in single–conductor transmission line. Two matrices F_1 and F_2 are introduced, which can be calculated easily from the measurements at the sending end. The simulation results give good agreement with the proposed algorithms. But invariably, some limitations exist. Theoretically, it is applicable for any point on the wave but computationally more expensive than the correlation technique, and it does require to know what type of fault is involved in order that the model mixing at the fault point be correctly incorporated. On the other hand. the system really has to be an ideal system with very low high–frequency noise and this limits its scope of application. Even the effect of the travelling waves will affect the result of the prediction algorithm and make it less effective. On the other hand, it does not work as well in close–up fault because a strong source behind the relaying station will inevitably change the shape of the wavefront. Maybe one would look at another example of a close–up fault at location 4.

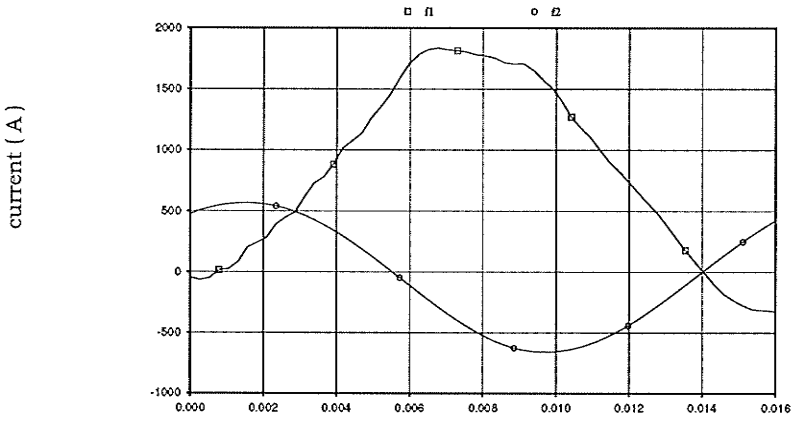

The wave function f1 and f2

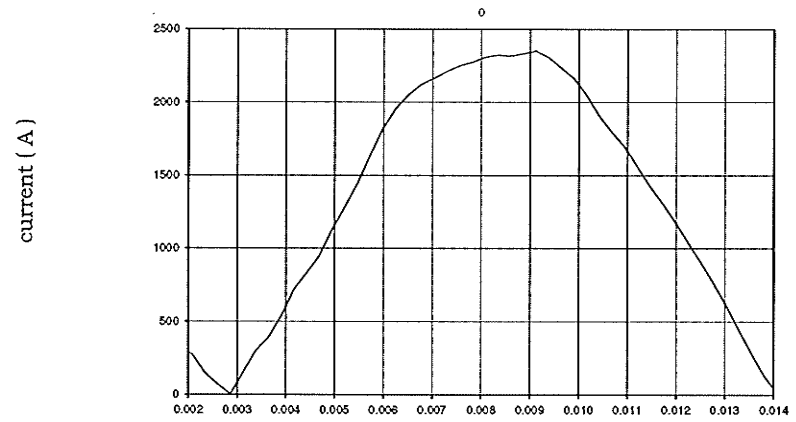

Difference between f1 and f2

Figure 4 .10 : Phase a to phase b fault at Pow 0 at location 4

The above figure shows a phase to phase fault at location 4 which is 88 km away from the relay station. The beginning of f1 shows some resemblance to the f2 signal especially at the top where the signal turns around. From the bottom figure we can find a ill–shaped platform where the difference comes to a nearly constant area and we can see that this area is about half a millisecond which is about 150 km, or twice the distance from relaying position to location 4. It seems we are having a difficulty in trying to define in what range the difference can be called a constant.

As we mentioned earlier, the waveform matching requires a very "clean " wave without noise because we have to match the waveform point by point. Any unexpected deviation will result in error in the relay judgement and has to be treated with caution.

Chapter 5
Comparison of the Algorithms

5.1 INTRODUCTION

As we can see in the previous chapters, all three algorithms have their special advantages in their applications and they all have some limitations in some particular situations. However, the response of each algorithm is robust in terms of the fault situation and it is obvious that the response is closely linked with the fault situation. It will be interesting to examine their individual behavior under the same fault situation. By studying the results from different algorithms, we can at least have some clue of what type of fault is involved and preferably, the location of the fault.

5.2 COMPARISON

First, let's look at a close–up fault situation. The fault is a phase to phase fault at location 4 which is 88 km away from the relay. The fault happens when one of the phases is at 0 POW. The responses of the three algorithms are shown in the following figures.

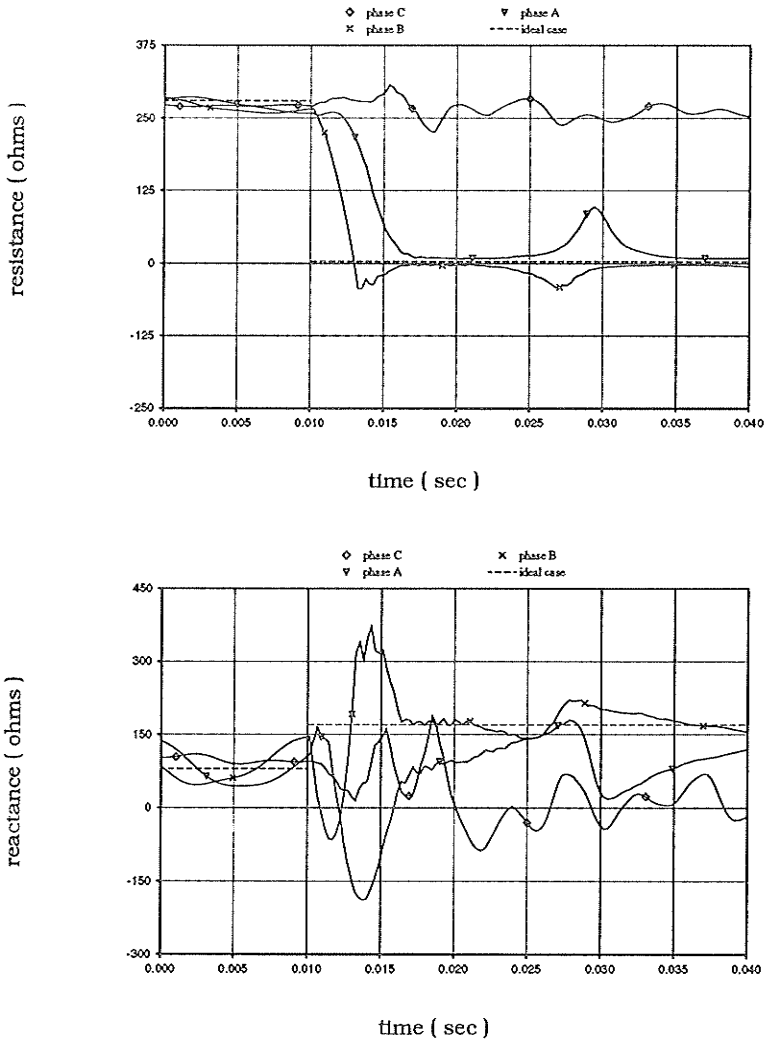

Figure 5 .1 : response of impedance measurement algorithm

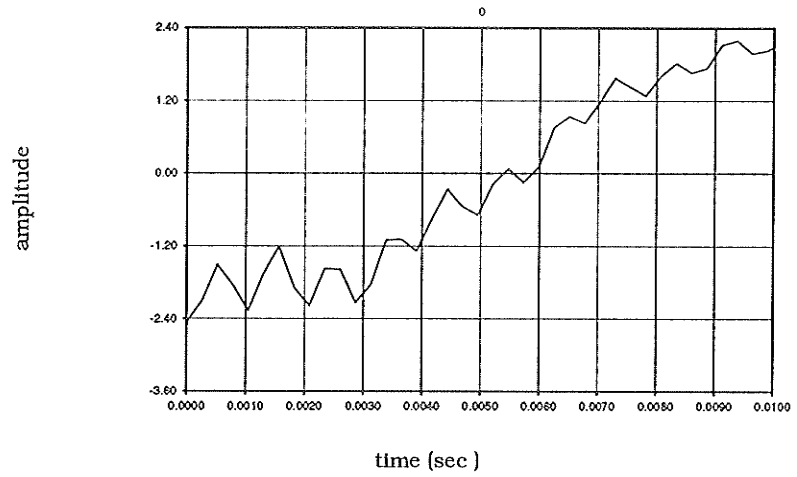

Figure 5 .2 : response of travelling wave correlation algorithm

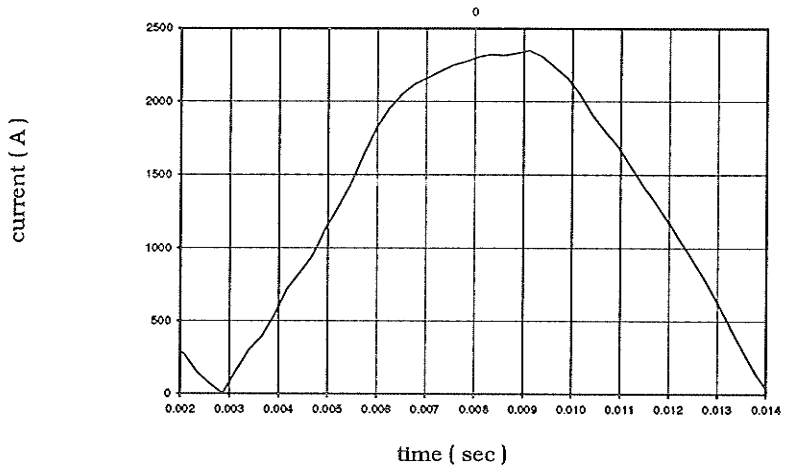

Figure 5 .3 : response of wavefront predicting algorithm

From fig 5.1 5.2 and 5.3, we can see that, in the impedance measurement algorithm, the resistance and reactance go to their steady value after about 30 ms (this is not very fast) and the new impedances of the two faulted phases are relatively attenuated. The travelling wave measurement algorithm also gives the peak at 0.5 ms which corresponds to 150 km (twice the distance to fault) but as in one phase the fault inception angle is zero, the magnitudes of the following peaks are bigger than the first, this will result in mal–function of the corresponding relay. The wavefront predicting algorithm doesn't function too well,

either. Because it is a close–up fault, the reflection of the source will affect the waveshape and we can not get a flat period in the signal |f1 – f2|. We can only see a rough ramp there which convinces us that there is something happening because the difference between two sinusoidal signals will still be sinusoidal unless one of the sinusoidal signals starts to change (i.e. a fault happens). But one can imagine that it is still very difficult to make a trip decision upon a ramp signal.

The next situation to consider is the situation when a single phase to ground fault happens at location 9 at inception angle of zero. The distance to the fault is about 260 km. The results are shown in fig5.4, 5.5, 5.6.

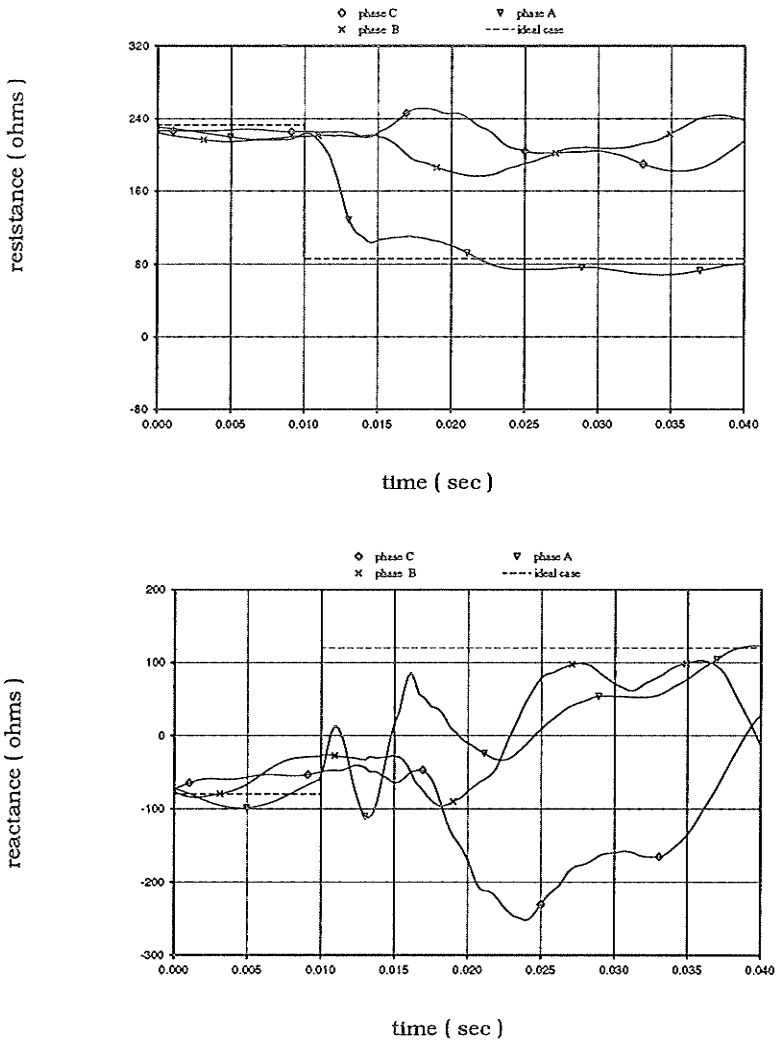

Figure 5 .4 : response of impedance measurement algorithm

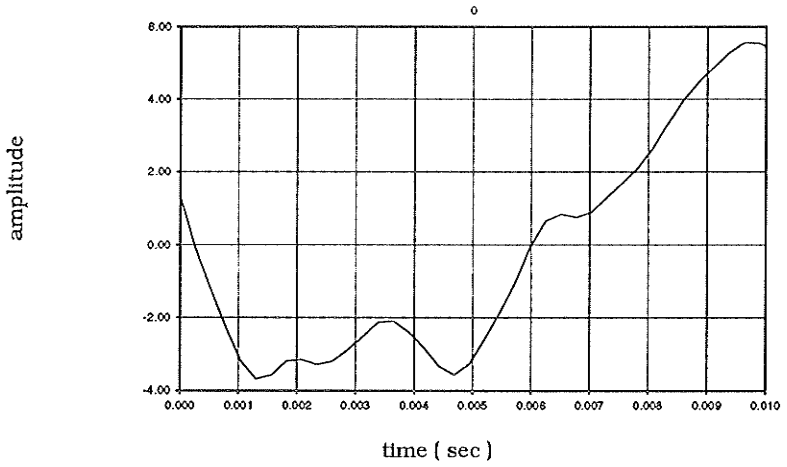

Figure 5 .5 : response of the travelling wave correlation algorithm

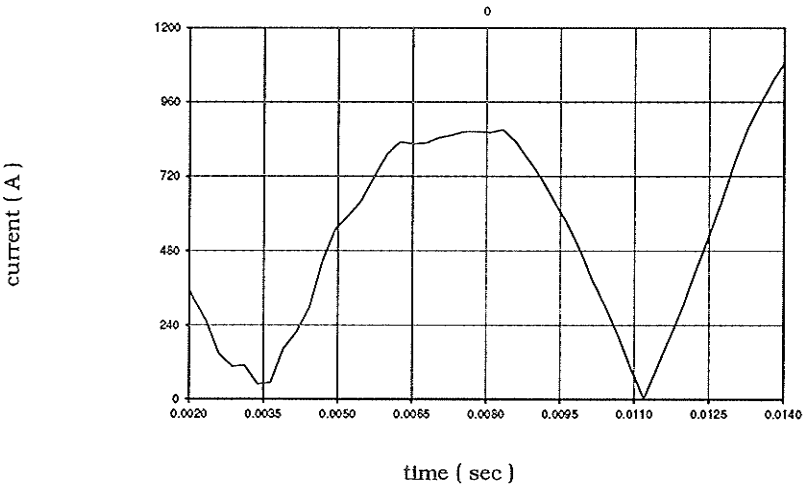

Figure 5 .6 : response of the wavefront predicting algorithm

This time the response of the impedance measurement algorithm will not converge. We can see after 30 ms the reactance still does not converge and we can see from the impedance trajectory that the impedance on the faulted phase shows signs of oscillation. The travelling wave algorithm also gives an unsatisfactory result because of the weak nature of the superimposed signal. However the wavefront prediction algorithm gives a correct response by showing a flat period in | f1 – f2 | signal which corresponds to the phase shift

of about 2 ms. This equals 600 km in distance, roughly twice the distance from the fault location to the relay.

The next case is slightly different from the previous example. The fault is a three line to ground fault at location 10 which is 290 km away from the relay. The results of each algorithm are shown in fig 5.7, 5.8.

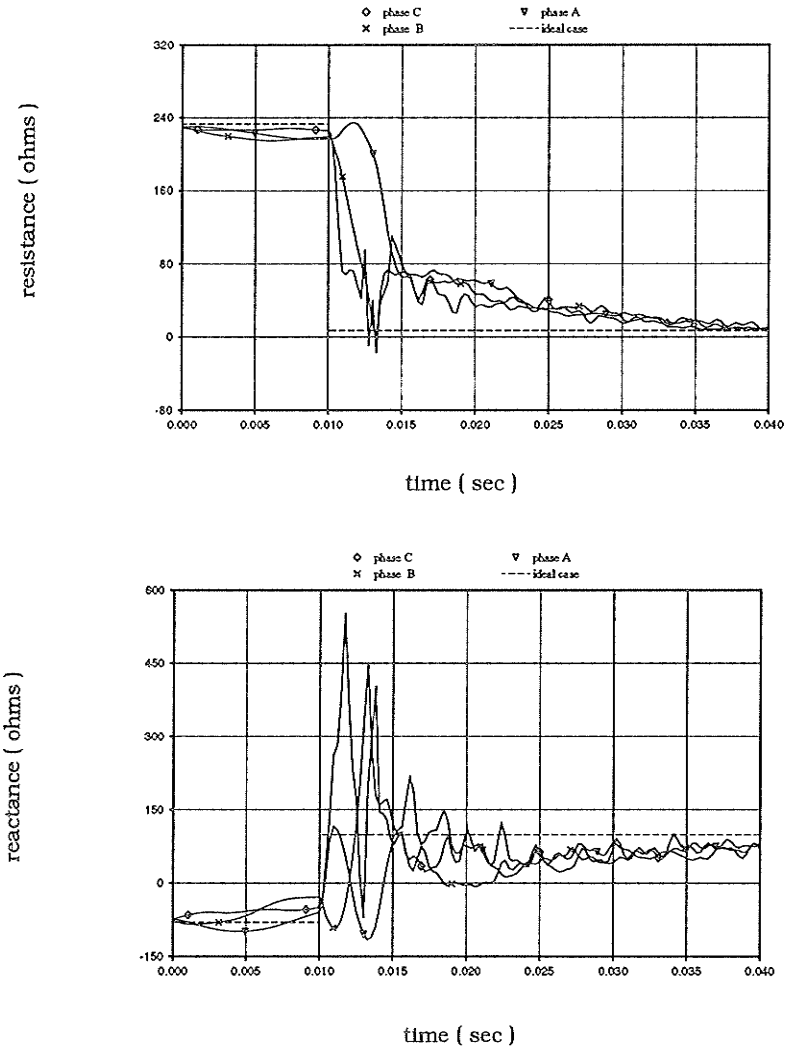

Figure 5 .7 : response of impedance measurement algorithm

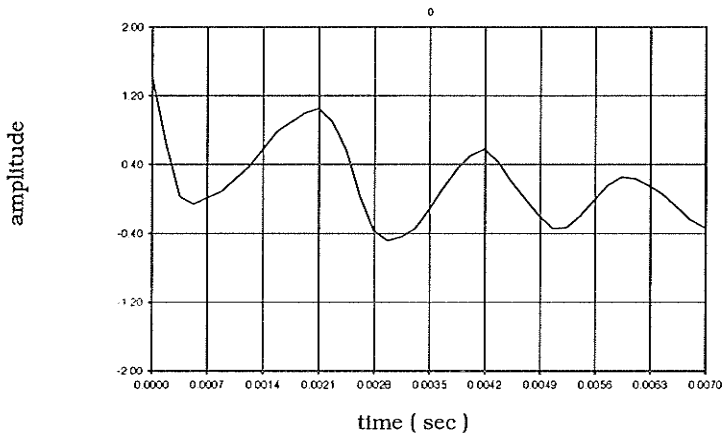

Figure 5 .8 : response of the travelling wave correlation algorithm

The figures show that the impedance measurement algorithm works much better, partly because we are dealing with a three phase to ground fault and the change in the signals are much stronger. We can see that the impedance in all three phase goes to its steady state value after about 15 ms, and the impedance trajectory shows a strong sign of convergence. The travelling wave algorithm also gives a correct result. It gives the first peak at 2.1 ms which corresponds to a distance of 630 km, roughly twice the distance between location 10 and the relay. The wavefront predicting algorithm can not work because the Clarke transformation is not able to distinguish three phase to ground fault.

The last case is a fault happening at location 7 which is 450 km away from the relay. It is a single line to ground fault.The difference is that the inception angle is now 60 instead of zero because we want to see how the wavefront prediction technique will behave in such a case.

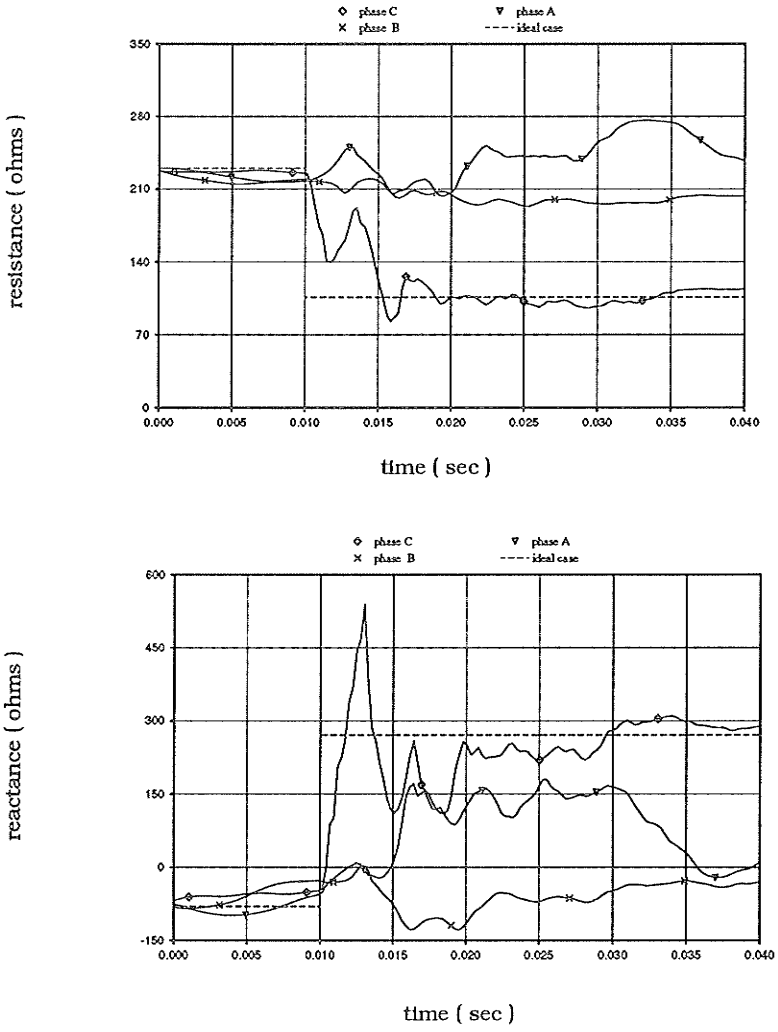

Figure 5 .9 : response from the impedance measurement algorithm

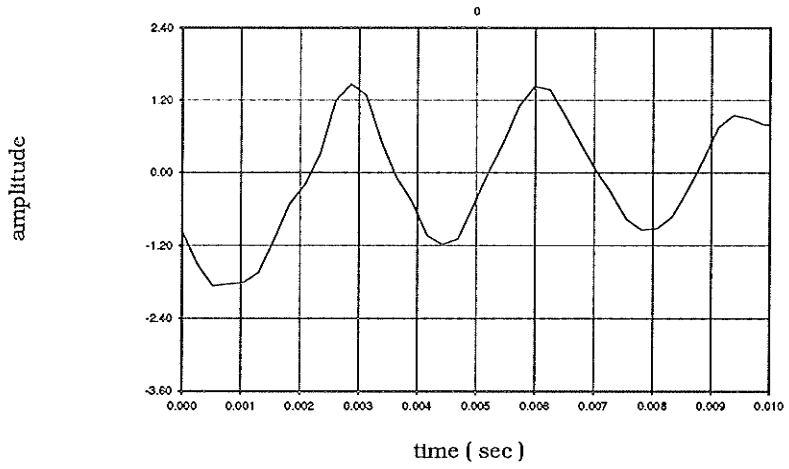

Figure 5 .10 : response from the travelling wave correlation algorithm

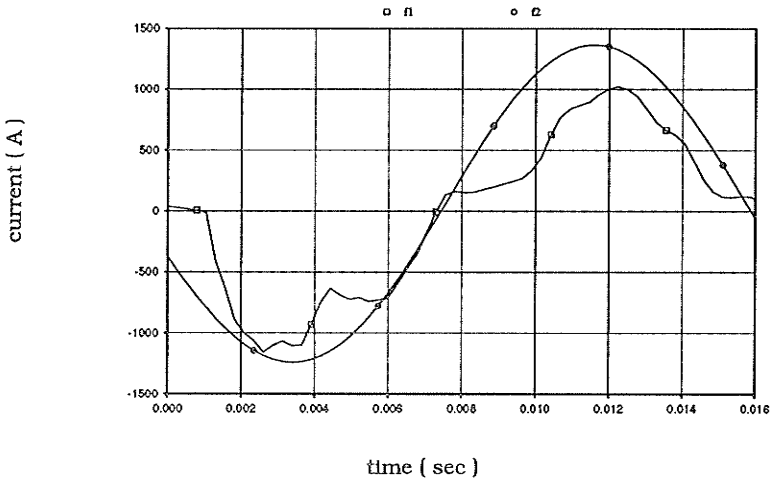

Figure 5 .11 : response of the wavefront predicting algorithm

The impedance measurement algorithm gives a slow response and the impedance trajectory shows that the impedance will not converge after 30 ms. The travelling wave algorithm gives out a correct response by indicating a peak at 3 ms which points out that the distance to fault is 450 km. This is exactly the distance from location 7 to the relay station. The wavefront predicting algorithm does not give any result simply because the magnitude of the travelling wave is too big and it affects the waveshape too much, there is no way we can tell the phase difference because the two signals are just too similar.

5.3 CONCLUSION

The case study in the previous section shows that, in the applications of the individual algorithms, two things are certain. First, each algorithm will have a robust response towards the fault signals and each algorithm caters for some special applications. Second, these responses overlap each other. These two features lay the ground work for a composite relaying system which is able to combine and compare the results of the three algorithms to reach a more reliable decision.

Due to the complexity of power transmission line systems, including different fault situations (type, inception angle, etc.) and system configurations, it is very difficult to define quantitatively the decision to trip based on the results of the three algorithms. But some basic rules apply, for instance, when the impedance measurement algorithm gives a stable result and the superimposed signal levels are high but neither the correlation algorithm nor the wavefront predicting algorithm gives a clear answer, the fault is most likely to be a close–up fault; when some signs of oscillation are shown in the impedance measurement algorithm and the correlation technique gives a well–defined peak, then the result of the correlation is more believable; when both correlation and impedance measurement techniques show some hesitation while the signal level is low and the wavefront predicting algorithm gives a clear flat peak, this probably reflects the true situation in the transmission line. Fortunately, the most common case is that at least two algorithms will overlap each other. So even if the result of one of the algorithm is hesitant, we can still determine what is happening. This requires that the result of each algorithm should always be procurable within a certain scope, and should not be just in the form of " trip " or " not trip ", which will certainly bring some advantage into the decision making stage.

Chapter 6
Implemetation

6.1 INTRODUCTION

All three algorithms (the short window impedance measurement algorithm, the travelling wave correlation algorithm, the waveshape predicting algorithm) are realized using software in C++ language on a Borland C 3.0 platform. The initial fault data were generated by EMTDC version 3. using the Dorsey–Forbes–Chisago transmission line model. The system configuration can be found in Fig 1.2 in Chapter 1. The line voltage and current are sampled at a rate of 640 samples per cycle, namely 38.4 kHz. After the fault voltage and current samples have been obtained, they are filtered through a low–pass filter which takes in the average of every 10 consecutive samples. The result we get is the pre–filtered samples and the sampling rate seen by the PC computer is 64 samples per cycle or 3.84 kHz, which is more convenient for processing on a PC level. The results are obtained by running the pre–filtered data samples through all three programs which can be plotted using EMTDC at a later stage. The complete listing of all the source codes of the three algorithms can be found in Appendix B.

6.2 FLOWCHARTS

The flowchart diagrams for all the three algorithms can be found in the following figures.

6.2.1 IMPEDANCE MEASUREMENT ALGORITHM

The flow chart for the impedance measurement algorithm can be represented in the following diagram:

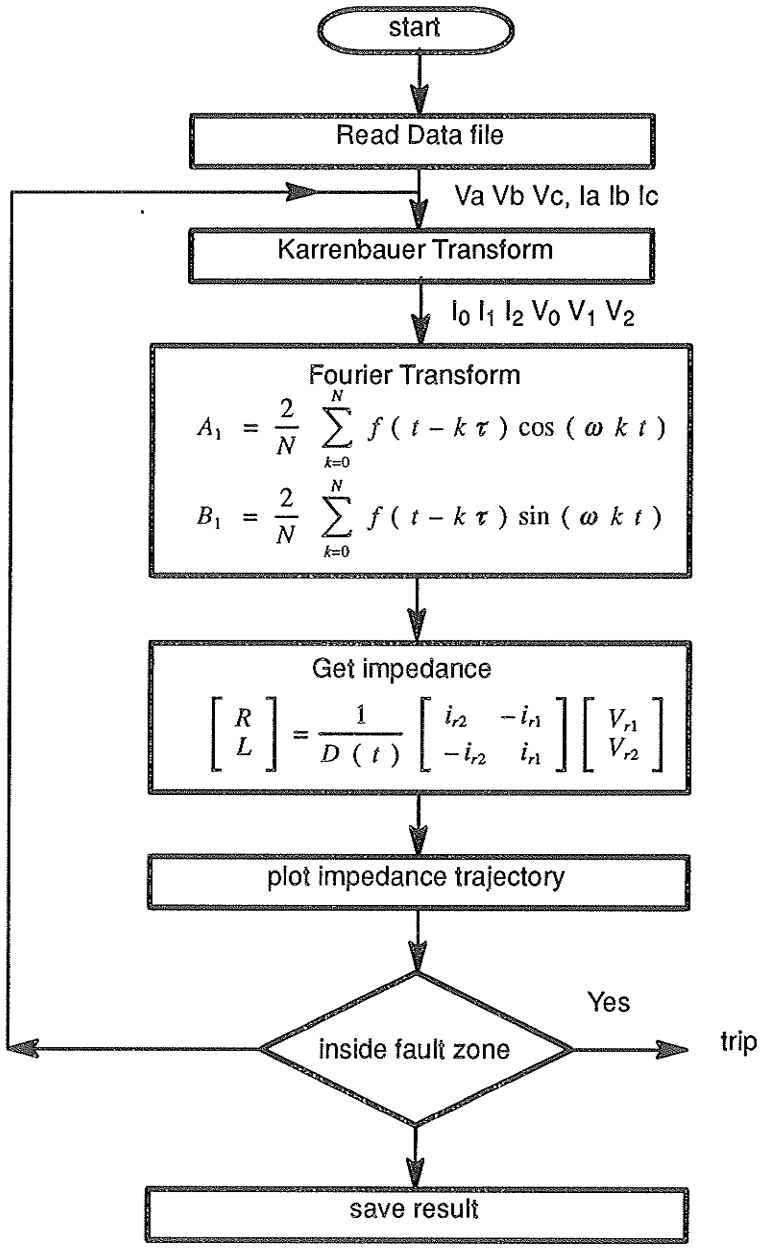

Figure 6.1 : flowchart for impedance measurement algorithm

6 .2 .2 TRAVELLING WAVE DISTANCE PROTECTION ALGORITHM

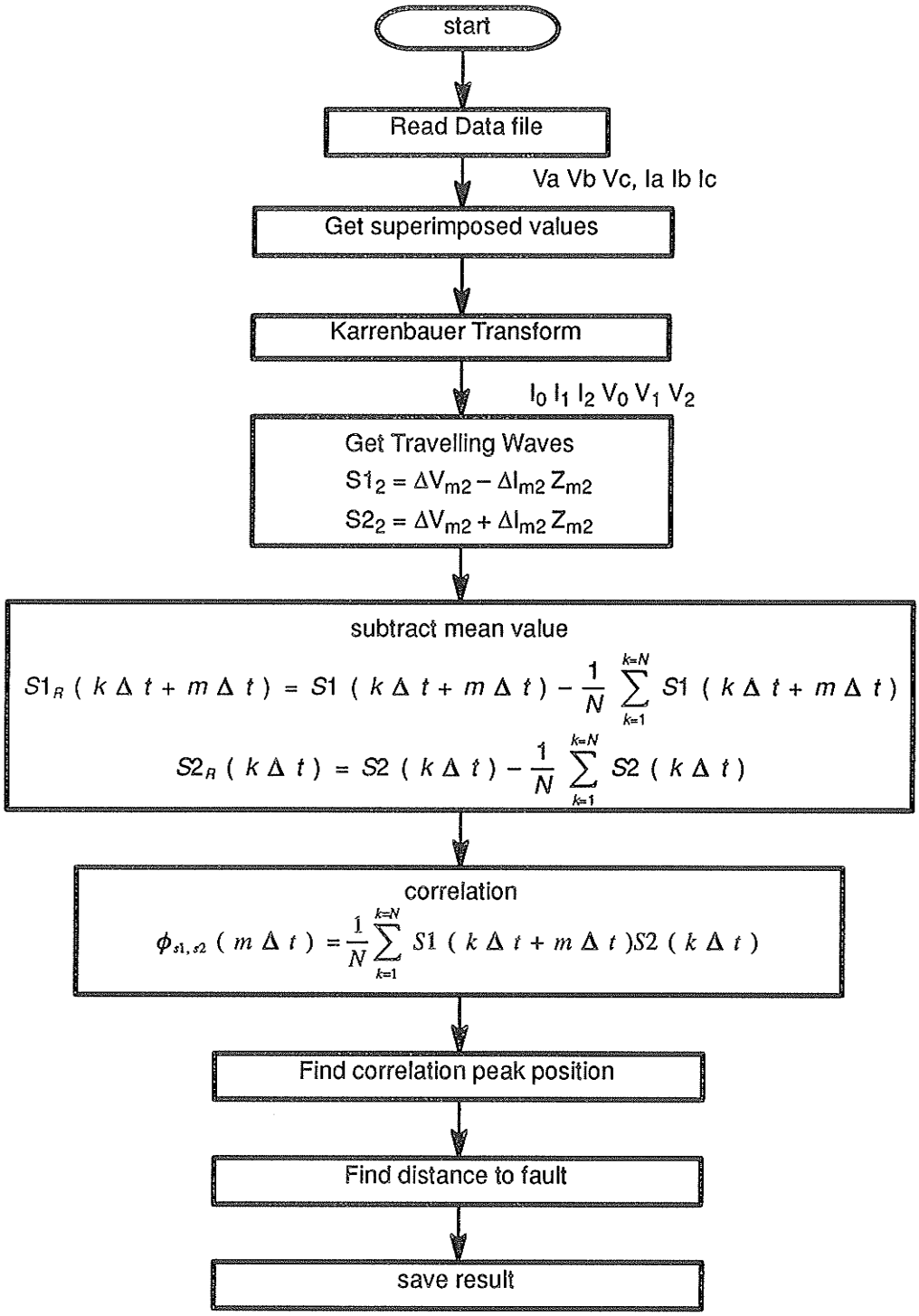

Figure 6 .2 : flowchart for the travelling wave algorithm

6 .2 .3 WAVEFRONT PREDICTION ALGORITHM

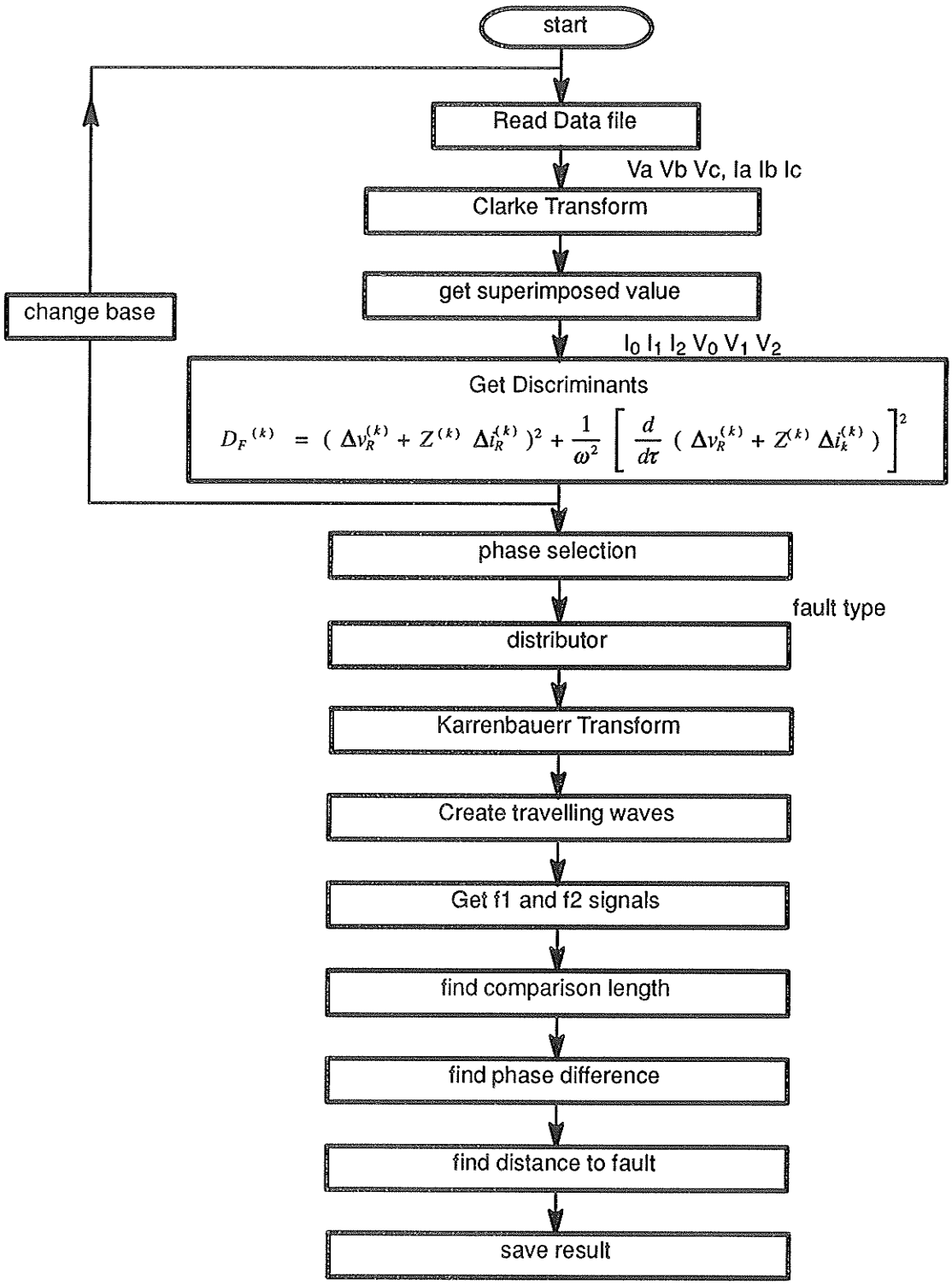

Figure 6 .3 : flow chart for the wavefront prediction algorithm

6.3 SOURCE CODES

All source code listings can be found in Appendix B.

Chapter 7
Decision Making and Conclusions

7.1 INTRODUCTION

There are three different protection techniques used. The short line algorithm is based on a 6.4 ms window and the extraction frequency used has a period of 6.4ms. When there is evidence of large wavefronts in the signals a correlation technique based on the a certain sampling window described in [5] is used. High speed fault location requires high sampling rates. When there are no significant wavefronts but the incremental signals indicate the presence of a disturbance then the waveshape predicting technique is employed to find out the fault distance. All three algorithms have their advantages and disadvantages in practical applications, and the results always vary according to different fault type, location and the configuration of the system. The results indicate that they overlap each other and thus it is necessary to look at the results in light of the fault situation and the algorithm that has been used so that right decisions can be reached.

7.2 COMPARING SIMULATION RESULTS

The output from all three techniques can be investigated to produce reinforcing information. The relationship between impedance and distance is linear for distance to fault

for which a lumped parameter model is appropriate. Such a distance is typically around 150 km at power frequency. On long lines, say 500 km, the remaining part of the zone 1 coverage up to 400km requires a different technique for accurate measurement of distance particularly so around the 400 km boundary.Long lines tend to be critical from a stability point of view and speed of detection for faults is an important factor in increasing stability margins. The remainder of the zone up to 400km is covered by travelling wave distance measurement based on a correlation technique to recognize wavefronts returning from the fault[3]. Should the fault occur at a point on wave giving very low levels of wavefront on the line then a new waveshape prediction technique based on the telegrapher's equations is used.

The concept of an estimate is important since it is necessary to model the system or the waveforms in order to develop an algorithm. As the system or waveforms do not exactly fit the assumed model, errors are introduced which lead to errors in the computed parameters. The response of the algorithms to these non–model signals is an important consideration in the selection of an algorithm.

From the results we can see that the impedance measurement algorithm is more stable when there are no substantial wavefronts on the system; if neither the correlation nor the waveshaping algorithm gives a well defined fault location but the incremental signals are high, then it is probably a close–up fault which the impedance measurement algorithm should measure accurately; if the correlation technique gives a good result indicating a strong correlation for the distance to the fault at some relatively long distance, then the impedance measurement algorithm is likely to have a difficult time to converge to its post–fault value and some kind of oscillation is likely to happen. If the magnitude of the superimposed signal is low and the correlation technique cannot give a good result, the waveshapes prediction technique will play the major role when we have enough evidence that a fault exists in the system. This is a further reinforcement of the basic measurement for the travel time to and from the fault from Dorsey.

7.3 CONCLUSIONS

From the above research, we can see that a parallel processing procedure running three different algorithm can be incorporated to detect a distance measurement technique on a long line. There are many features in the output of each algorithm which can be used to reinforce the result from the algorithm which is most accurate for the particular distance in question and a fuzzy logic control modal will be required to process these results in order to get a correct decision.

The conclusion we can obtain is that each algorithm has its own advantages and disadvantages. The short window impedance measurement scheme is more accurate when we talk about short line protection; the travelling wave algorithm is faster in terms of the response and the distance to fault can be found at the same time, but it works better with long lines and the accuracy is greatly affected by the fault inception angle and the other discontinuities along the line; the wavefront prediction technique is a good complement to the travelling wave algorithm in that it helps to tell the incident wavefront of the faulted signals before they arrive. All three schemes combined together can offer a much larger coverage of the power system network. Laboratory experimental results of these three schemes have shown the advantages offered by each so that we can begin to envision a more reliable protection system in which the three schemes work simultaneously, each with its individual merits, but on a combination basis. In spite of the fact that the cost of such a centralized protection system can be a little bit more expensive, and that we still cannot make it run in real time owing to the limitation in the processing speed of the available hardware, we believe that in the near future, using cheaper and faster processing chips, we could make such a system into a reality to achieve better protection performance in the power system.

Appendix

This appendix is intended to give a comprehensive result of the fault condition matrix and construct corresponding F_1 and F_2 in accordance with different fault types in the application of wavefront predicting algorithm.

As has been stated in the Chapter 4, the fault condition can be expressed by the following admittance–matrix at the fault position

$$Y_p = \begin{bmatrix} y_{aa} & y_{ab} & y_{ac} \\ y_{ba} & y_{bb} & y_{bc} \\ y_{ca} & y_{cb} & y_{cc} \end{bmatrix}$$

where y_{aa}, y_{ba}, .. etc. are the fault resistance between phases or between phase to ground. Thus when we want to express a certain type of fault, we can just let the related phase to be the fault resistance, and let those admittance at non related phase to be zero. For instance, for a phase C to phase A fault, the fault admittance matrix can be expressed as :

$$Y_p = \begin{bmatrix} y_{ac} & 0 & y_{ac} \\ 0 & 0 & 0 \\ y_{ca} & 0 & y_{ca} \end{bmatrix}$$

Thus the fault modal admittance matrix can be expressed by

$$Y_m = S^{-1} Y_p S$$

The fault condition matrix, according to the equation 4.29

$$A = 2\, Y_0\, Y_{mn}^{-1} - I$$

where

$$Y_{mm} = 2\, Y_0 + Y_m = 2 \begin{bmatrix} y_{0\gamma} & 0 & 0 \\ 0 & y_{0\alpha} & 0 \\ 0 & 0 & y_{0\beta} \end{bmatrix} + Y_m$$

Now we can start calculating the fault condition matrix in all sorts of cases, keep in mind that we shall neglect fault resistance because they are much smaller than the surge impedance. As a result, all the matrices converge to its ideal form when we assume that the corresponding fault admittance to be infinite.

(1) for phase A to ground fault

$$A = \frac{-1}{a+b+c}\begin{bmatrix} a & b & c \\ a & b & c \\ a & b & c \end{bmatrix}$$

(2) for phase B to ground fault:

$$A = \frac{-1}{a+2b}\begin{bmatrix} -a & 2b & -c \\ a & -2b & c \\ 0 & 0 & 0 \end{bmatrix}$$

(3) for phase C to ground fault :

$$A = \frac{-1}{a+2c}\begin{bmatrix} -a & -b & 2c \\ 0 & 0 & 0 \\ a & b & -2c \end{bmatrix}$$

(4) for phase A to phase B fault :

$$A = \begin{bmatrix} 0 & 0 & 0 \\ 0 & -1 & 0 \\ 0 & -0.5 & 0 \end{bmatrix}$$

(5) for phase B to phase C fault:

$$A = \frac{1}{b+c}\begin{bmatrix} 0 & 0 & 0 \\ 0 & -b & c \\ 0 & b & -c \end{bmatrix}$$

(6) for phase A to phase C fault:

$$A = \begin{bmatrix} 0 & 0 & 0 \\ 0 & 0 & -0.5 \\ 0 & 0 & -1 \end{bmatrix}$$

Rewrite equation 4.32, note in steady state the ground mode components of the modal signals are equal to zero.

$$\begin{bmatrix} S_{1\gamma}(t+\tau) \\ S_{1\alpha}(t+\tau) \\ S_{1\beta}(t+\tau) \end{bmatrix} = A \begin{bmatrix} 0 \\ \hat{I}_{1\alpha}(t+\tau) + \hat{I}_{2\alpha}(t+\tau) \\ \hat{I}_{1\beta}(t+\tau) + \hat{I}_{2\beta}(t-\tau) \end{bmatrix}$$

Signal F_1 and F_2 now can be obtained using equation

$$F_1(t) = S_1(t+\tau) - A\, I_1(t+\tau)$$

$$F_2(t) = A\, I_2(t-\tau)$$

Wave function F_1 and F_2 in accordance with different fault types are listed below.

(1) for phase A to ground fault

$$f_{1\alpha} = S_{1\alpha} + \frac{1}{a+b+c}\left[b\,\hat{I}_{1\alpha}(t) + C\,I_{1\beta}(t)\right]$$

$$f_{2\alpha} = -\frac{1}{a+b+c}\left[b\,\hat{I}_{2\alpha}(t) + C\,I_{2\beta}(t)\right]$$

(2) for phase B to ground fault

$$f_{1\alpha} = S_{1\alpha} + \frac{1}{a+2b}\left[2\,b\,\hat{I}_{1\alpha}(t) - c\,\hat{I}_{1\beta}(t)\right]$$

$$f_{2\alpha} = -\frac{1}{a+2b}\left[2\,b\,\hat{I}_{2\alpha}(t) - c\,\hat{I}_{2\beta}(t)\right]$$

(3) for phase C to ground fault

$$f_{1\beta} = S_{1\alpha} + \frac{1}{a+2c}\left[b\,\hat{I}_{1\alpha}(t) - 2\,c\,\hat{I}_{1\beta}(t)\right]$$

$$f_{2\beta} = -\frac{1}{a+2c}\left[b\,\hat{I}_{2\alpha}(t) - 2\,c\,\hat{I}_{2\beta}(t)\right]$$

(4) for phase A to phase B fault

$$f_{1\alpha} = S_{1\alpha} + \hat{I}_{1\alpha}(t)$$

$$f_{2\alpha} = -\hat{I}_{2\alpha}(t)$$

(5) for phase B to phase C fault

$$f_{1\alpha} = S_{1\alpha} + \frac{1}{b+c}\left[b\,\hat{I}_{1\alpha}(t) - c\,\hat{I}_{1\beta}(t)\right]$$

$$f_{1\alpha} = \frac{1}{b+c}\left[-b\,\hat{I}_{1\alpha}(t) + c\,\hat{I}_{1\beta}(t)\right]$$

(6) for phase A to phase C fault

$$f_{1\alpha} = S_{1\alpha} + \frac{1}{2}\,\hat{I}_{1\beta}(t)$$

$$f_{2\alpha} = -\hat{I}_{2\beta}(t)$$

REFERENCES

[1] P.A.Crossley and P.G. McLaren, " Distance Protection based on Travelling Waves ", IEEE Trans. PAS, Vol. PAS– 102, No. 9, Sept. 1983, p. 2971.

[2] EMTDC User's Manual, Manitoba HVDC Research Centre, November 1988.

[3] P.G. McLaren and Y.P. Wang, " High Speed Relaying on Long EHV AC Transmission Lines ", Proc. of Canadian Conference on Electrical and Computer Engineering, Ottawa, Canada, Sept. 4–6, 1990, Vol. 1, pp. 1.3.1 – 1.3.4.

[4] M. Vitins, " A Correlation Method for Transmission Line Protection ", IEEE Trans. PAS, Vol. PAS– 97, No. 5, Sept/Oct. 1978, pp. 1607 – 1617.

[5] P. Agrawal, " An Investigation into A Method of Detecting the Fault Induced High Frequency Voltage Signals of EHV Transmission Lines for Protection Applications ", IEEE / PES 1990 Summer Meeting, Minneapolis, July 15 –19, 1990.

[6] Y. V. V. S Murry and W. J. Smolinski, " A Kalman Filter Based Digital Percentage Differential and Ground Fault Relay For a 3 – Phase Power Transformer ", IEEE Trans on Power Delivery, Vol 5. No 3, July 1990.

[7] M. M. Giray and M. S. Sachdev, " Off – Nominal Frequency Measurements in Electric Power Systems ", IEEE Trans on Power Delivery, Vol 4. No 3, July 1989.

[8] A.T. Johns and R.K. Aggarwal, " Digital Simulation of faulted EHV Transmission Lines with Particular Reference to Very–high–speed Protection ", Proc. IEE. Vol. 123, No. 4, April, 1976, pp. 353 – 359.

[9] M.M.S. Mansour, " A Travelling Wave Relay Featuring Fault Classification and Phase Selection ", Ph. D. Thesis. Dept. of Electrical Engineering, Univ of Manitoba. Winnipeg, Canada, 1984.

[10] A.T. Johns and M.A. Martin, " New Ultra High Speed Distance Protection Using Finite Transform Techniques ", Proc. IEE, Vol 130, Part C, No.3, May 1983, p127.

[11] E.S. Shehab–Eldin, P.G. McLaren, " Travelling Wave Distance Protection – Problem Areas and Solutions ", IEEE Trans on Power Delivery, Vol. 3, July 1988, p990.

[12] P.G. McLaren and M.A. Redfern, " Fourier Series Techniques Applied To Distance Protection ", Proc. IEE, Vol. 122, 1975, p1301.

[13] H.W. Dommel, J.M. Michels, " High Speed Relaying using Travelling Wave Transient Analysis ", IEEE PES Winter meeting, New York 1978, paper no. A78 214 – 9.

[14] D.W.P. Thomas and C. Christopoulos, " Ultra – High Speed Protection of Series Compensated Lines ", IEEE PES 1991 Summer Meeting, San Diego, California, July 28 – August 1, 1991.

[15] J.G. Kappenman, G.A. Sweezy, V. Koschik and K.K. Mustaphi, "Staged fault tests with single phase reclosing on the Winnipeg–Twin cities 500kV interconnection," IEEE Transactions on Power Apparatus and Systems, Vol. PAS–101, No. 3 March 1982.

[16] A.D. McInnes and I.F. Morrison, " Real time calculation of resistance and reactance for transmission line protection by digital computer ", IEEE Trans. PAS, Vol. 79, No. 5, pp. 1546–1551, October 1979

[17] F. Engler, O.E. Lanz, M. Hanggli and G. Bacchini, " Transient signals and their processing in an ultra high speed directional relay for ehv/uhv transmission line protection", IEEE Trans. PAS, Vol. 104, June 1985, P. 1463

[18] A. O. Ibe and B. J. Cory, " A travelling–wave based faultlocator for two and three terminal networks", IEEE Trans. PAS, Vol. PWRD–1, No. 2, 1986

[19] Y. M. Ko, "Single ended high speed distance relay based on travelling wave phenomenon", P.hD Thesis UMIST, Manchester 1980.

[20] Fallou, J. A, "Propagation des courants de haute frequence poly–phases le long des lignes aeriennes de transport d'energie affectees de courts–circuits ou de defauts d'isolement" Bull. Soc.Franc.Elect., 1932, Series 5, 2, P.787